# Thermodynamics of Sorption and Distribution of Water in Nafion

by

Gwynn Johan Elfring
B.Eng., University of Victoria (2005)

A Thesis Submitted in Partial Fulfillment of the
Requirements for the Degree of

MASTER OF APPLIED SCIENCE

in the Department of Mechanical Engineering

Supervisory Committee:

_____

Dr. Henning Struchtrup, Supervisor (Mechanical Engineering)

_____

Dr. Nedjib Djilali, Department Member (Mechanical Engineering)

_____

Dr. David Sinton, Department Member (Mechanical Engineering)

_____

Dr. David Harrington, External Examiner (Chemistry)

Supervisor: Dr. Henning Struchtrup

## Abstract

In this work a model for the wetting and swelling of pores with water within a Nafion membrane is developed. This model is based on minimizing all contributions to the total free energy of the proposed system. We find that equilibrium state depends on entropic mixing forces and energetic surface forces. The wetting of the pore relies on the entropic forces exceeding the energetic forces. Specifically this indicates a critical pore size in which liquid is the favorable state. If the pore fills with liquid it will swell until balanced by the energy of the deforming membrane. Several factors including pressure relative to saturation and the phase which bounds the membrane are shown to dramatically affect the final equilibrium state of the system.

Supervisory Committee:

_____

Dr. Henning Struchtrup, Supervisor (Mechanical Engineering)

_____

Dr. Nedjib Djilali, Department Member (Mechanical Engineering)

_____

Dr. David Sinton, Department Member (Mechanical Engineering)

_____

Dr. David Harrington, External Examiner (Chemistry)

# Table of Contents

# List of Figures

## Nomenclature

| | |
|---|---|
| $a_\theta$ | end area function (1) |
| $A$ | area $\left(m^2\right)$ |
| $A_c$ | area of cylinder $\left(m^2\right)$ |
| $A^c$ | area constant $\left(m^2\right)$ |
| $A_{end}$ | area of end $\left(m^2\right)$ |
| $b_\theta$ | end volume function |
| $C$ | parameter to vary $S_p$ (1) |
| $f$ | specific Helmholtz free energy $(J/kg)$ |
| $f_{end}$ | energy of ends $(J)$ |
| $F$ | Helmholtz free energy |
| $F_{el}$ | elastic energy of membrane $(J)$ |
| $g$ | specific Gibbs free energy $(J/kg)$ |
| $G_{mix}$ | Gibbs free energy of mixing $(J)$ |
| $G^E_{mix}$ | excess Gibbs free energy of mixing $(J)$ |
| $\mathcal{G}$ | total free energy of the system $(J)$ |
| $k$ | Boltzmann constant $\left(1.381 \times 10^{-23}\ J/K\right)$ |
| $K$ | equilibrium constant (1) |
| $L$ | length of liquid agglomeration $(m)$ |
| $L_t$ | length of pore $(m)$ |
| $m$ | mass $(kg)$ |
| $M$ | molar mass $(kg/mol)$ |
| $N$ | number of molecules (1) |
| $p$ | pressure $(Pa)$ |

| | |
|---|---|
| $p_{mix}$ | pressure of liquid water and proton mixture $(Pa)$ |
| $p_r$ | pressure ratio (1) |
| $p_{sat}$ | saturation pressure $(Pa)$ |
| $r$ | radius of liquid agglomeration $(m)$ |
| $r_0$ | unswollen pore radius $(m)$ |
| $r_c$ | critical pore radius for the stability of liquid water $(m)$ |
| $R$ | specific gas constant $\left(J \cdot kg^{-1}K^{-1}\right)$ |
| $R_u$ | universal gas constant $\left(8.314\ J \cdot mol^{-1}K^{-1}\right)$ |
| $S_p$ | surface density of protons $\left(m^{-2}\right)$ |
| $t$ | time $(s)$ |
| $T$ | temperature $(K)$ |
| $v$ | specific volume $\left(m^3/kg\right)$ |
| $V$ | volume $\left(m^3\right)$ |
| $V_c$ | volume of cylinder $\left(m^3\right)$ |
| $V_{end}$ | volume of end $\left(m^3\right)$ |
| $V_m^T$ | total volume of membrane $\left(m^3\right)$ |
| $X$ | mole fraction (1) |

**Greek**

| | |
|---|---|
| $\alpha$ | linear deformation factor (1) |
| $\beta$ | $S_p M_w/\rho_w\ \left(m^{-2}\right)$ |
| $\gamma$ | interfacial tension $\left(J/m^2\right)$ |
| $\gamma^a$ | activity coefficient (1) |
| $\theta$ | contact angle $(rad)$ |
| $\lambda$ | water molecules per sulfonate site (1) |

| | |
|---|---|
| $\lambda_C$ | strongly bound waters (1) |
| $\lambda_F$ | free waters (1) |
| $\mu$ | chemical potential $(J/kg)$ |
| $\nu_e$ | effective number of chains in the polymer network (1) |
| $\xi$ | $\beta^{-1}$ $\left(m^2\right)$ |
| $\rho$ | mass density $\left(kg/m^3\right)$ |
| $\phi$ | porosity of membrane (1) |
| $\chi$ | interaction parameter (1) |

## Subscripts

| | |
|---|---|
| $l$ | liquid |
| $lv$ | liquid-vapor |
| $m$ | membrane |
| $p$ | proton |
| $s$ | surface |
| $sl$ | solid-liquid |
| $sv$ | solid-vapor |
| $v$ | vapor |
| $w$ | water |

## Superscripts

| | |
|---|---|
| 0 | unswollen vapor filled reference state |
| $T$ | total quantity |

## Acknowledgements

First and foremost I'd like to thank my parents for basically forcing me into an education despite my efforts to sabotage them at every turn. If I hadn't tried to please them early in life I would never had been pleased with myself later in life, and in the end I think that was their plan all along.

Three educational figures really helped shape my desire to learn when so often my will to rebel against any form of structure whatsoever hindered my progress with so many others. I'd like to thank my middle school mathematics teacher Mr. Docherty who once told me he thought I was smart (which encouraged me at the time) and my high school chemistry teacher Mr. Clark who told me I was not as smart as I thought (which I invariably needed at the time). The third is my supervisor Henning Struchtrup. I drifted through my first couple of years of university in a haze of disinterest and inherently, mediocrity. School was like music that you can tolerate or even appreciate, but doesn't really speak to you. Henning's thermodynamics lectures spoke to me and instilled a deep passion for the beautiful theory behind it all. I've never had a question of Henning which wasn't but a few scratches of his pencil away from resolution and you can not ask much more from a supervisor than that.

And of course I thank Tracy, who allows me to spend fourteen hour days holed up in my bomb shelter office without developing a deep depression; Tracy, whom I love even more than thermodynamics.

# Chapter 1

# Introduction

With an ever increasing awareness of the hazards of global warming, alternative fuels and their applications have been receiving more public awareness. Fuel cells have the potential to dramatically impact carbon emissions by replacing many existing fossil fuel dependant technologies; however, we have yet to see a large scale adoption of fuel cell technology. Invariably the reasons are multifaceted; nevertheless, some of it still comes down to science. Fuel cells are very complex and the focus of intense academic research but fundamental insights are yet to be had if fuel cells and hydrogen are to be the way of the future.

A fuel cell offers a means to harness the difference in energy when hydrogen and oxygen are combined to form water. In a polymer electrolyte membrane (PEM) fuel cell, a polymer membrane, usually Nafion, separates the two reactants. The hydrogen gas is oxidized on the surface of the electrolyte into protons and electrons. The oxidation reaction is catalyzed by the presence of platinum particles. The membrane acts as an electronic insulator, but allows protons to pass. The electrons are given a path through which they perform work such as powering an electric motor. The reaction is completed as the electrons are diverted to the anode side of the membrane where they react with the protons and oxygen to form water (see Figure 1.1) [1]. The level of protonic mobility in the membrane is a function of the level of water content. As water content increases there is a greater interconnection of the liquid phase in the membrane. Bulk water offers extremely high protonic conductivity and as water content increases, polymer electrolyte membranes attain more bulk-like transport characteristics [2]. It is therefore critical

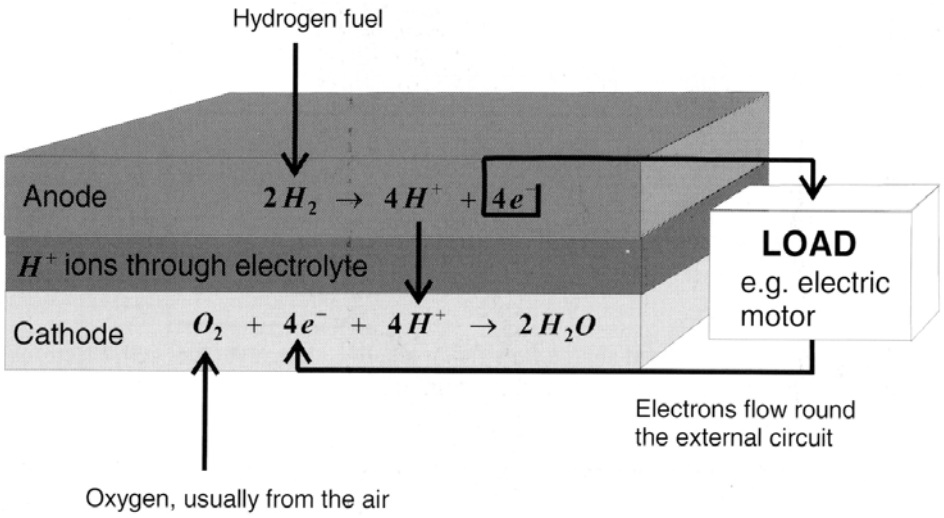


Figure 1.1: Hydrogen-Oxygen Fuel Cell Diagram [1].

to examine the nature of water uptake in a PEM.

In this work we study the sorption of water, in a Nafion membrane in particular, as it is the most commonly researched ionomer in the literature due to its excellent thermal, chemical and mechanical stability and wide commercial availability [3]. In this section physical characteristics of Nafion which affect the sorption of water and transport of protons are detailed.

## 1.1 Nafion Chemical Structure

Nafion is a perfluorosulfonate ionomer (PFSI); it is comprised of a polytetrafluoroethylene (PTFE) backbone (or matrix), and side chains ending in sulfonic acid groups, see Fig. 1.2 [4]. The PTFE backbone of Nafion is hydrophobic, while the acid groups attract water which leads to a high degree of phase separation in hydrated membranes. The counterion of the sulfonate group is predominantly $H^+$; however, depending on pretreatment it may also be $Na^+$ and $K^+$ [5]. A common form is Nafion 117 which has an equivalent weight (EW) of 1100 grams of dry Nafion per mole of sulfonic acid groups and has a nominal thickness of 0.007 inches [6]. Nafion

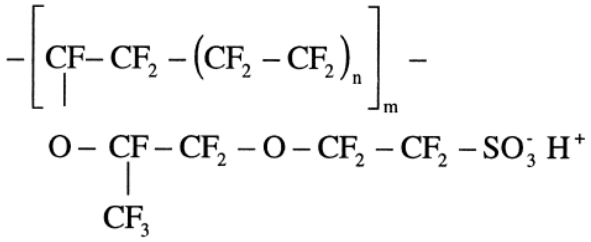

Figure 1.2: Nafion chemical structure [4].

115 and Nafion 112 are also widely available forms.

Spectroscopy studies performed by Zecchina et al. have shown that exposing the -$SO_3H$ acid groups in the Nafion membrane to water leads to a decrease in the number of such groups with a corresponding increase in the number of -$SO_3^-$ groups [7]. This is caused by the formation of $H^+(H_2O)_n$ groups as the proton dissociates from the acid group and bonds to one or more water molecules which are in turn strongly electrically attracted to the -$SO_3^-$ group. The protons do not return to the -$SO_3^-$ groups even after desorption past initial levels. This indicates that there is a high level of thermodynamic stability associated with the dissociation of the acid groups in water [7].

In a hydrated Nafion membrane, liquid is a mixture of water and $H^+(H_2O)_n$ ions. The entropy of mixing alters the chemical potential from the of the bulk saturated liquid or vapor at the boundaries of the membrane. This difference in chemical potential in turn draws more water into the membrane. As the membrane takes up water it swells to accommodate the solvent. The membrane backbone, however, is hydrophobic. The swelling of a polymer network in a solvent is typically viewed as a competition between the osmotic and elastic pressures which balance in equilibrium [8]. This equilibrium depends on whether there is saturated vapor or saturated liquid at the boundary of the membrane because a liquid-vapor interface is an additional force opposing water uptake. This difference is known as Schroeder's paradox [9].

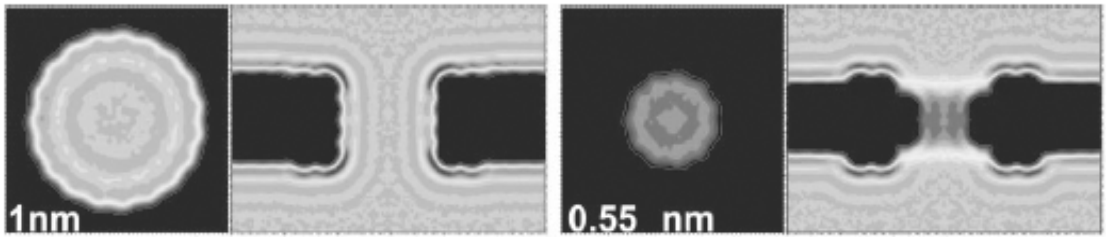


Figure 1.3: Evaporation in Nanopores [12].

## 1.2 Water in Hydrophobic Confinement

When water is confined by hydrophobic surfaces as it is in Nafion, one observes a critical separation distance at which the vapor becomes thermodynamically favorable. When confined by hydrophobic surfaces at a separation below the critical value, liquid becomes unstable and evaporates. It is suggested that a vapor film forms on the hydrophobic surfaces because the surface-particle attraction is so small that the attraction from the bulk effectively pulls the particle away from the surface [10]. There have been extensive experiments carried out by Christenson et al. documenting the cavitation of liquid water confined by hydrophobic surfaces [11]. They find that as two hydrophobic surfaces immersed in liquid water are brought together evaporation occurs. Christenson et al. conclude that since the interfacial free energy of a hydrophobic surface is lower against vapor than against water, it is energetically favorable for liquid water to evaporate, and thus the free energy of the system is minimized [11]. Similar results were found by Beckstein and Sansom when conducting molecular dynamics (MD) simulations of water in hydrophobic nanopores [12]. Figure 1.3 shows liquid in a 1 nm pore; however, in the 0.55 nm pore a decrease in the density of the fluid is observed, which approaches that of vapor. Oscillations between the two states occur by capillary evaporation and condensation, which are driven by small pressure variations in the bulk. Granick et al. carried out experiments confining liquid water between a hydrophilic surface and a hydrophobic surface [13]. They found a very dynamic response in both the spatial and shear dimensions of the

fluid. They concluded that such a response indicates that a vapor film forms on the surface of the hydrophobic material. This physical phenomenon is important when one considers the morphology of Nafion, in particular the hydrophobicity of the fluorocarbon backbone and the hydrophilicity of the sulfonate acid groups.

## 1.3 Nafion Proton Conductivity

The protonic conductivity of Nafion is of primary interest in fuel cell applications. Protons have a much higher level of conductivity in water than other ions; therefore, it is informative to observe the behavior of water in the presence of a protonic 'defect'. The dominant intermolecular interaction in water is hydrogen bonding [14]. The binding power of a water molecule depends on the number of hydrogen bonds it is involved in. For water at low temperature there is a well connected hydrogen bond network in water and as a result the activation energy to break a single bond is less than a third that of the average hydrogen bond energy; this leads to the rapid breaking and forming of hydrogen bonds. With the introduction of a proton a hydronium ion, $H_3O^+$, forms. The hydronium ion becomes hydrated by three neighbouring water molecules to form what is known as an Eigen ion, $H_9O_4^+$. The proton may also find itself as part of a dimer in the form of a Zundel ion, $H_5O_2^+$. Both configurations appear with equal probability and oscillate between each other on the order of $10^{-13}$ s, forming various intermediate structures in the process (see Figure 1.4) [14].

As the proton fluctuates between Zundel and Eigen configurations, it can facilitate spatial diffusion of the proton. This structural diffusion mechanism is known as the Grotthuss mechanism. One can visualize this diffusion in Figure 1.4, if the same proton is translated horizontally through the fluctuation of ionic species. In bulk water proton diffusion occurs primarily by the Grotthuss mechanism [14], but also occurs by traditional mass diffusion [15]; both mechanisms combined give water a high protonic conductivity. In the bulk, there are no set fixed and free

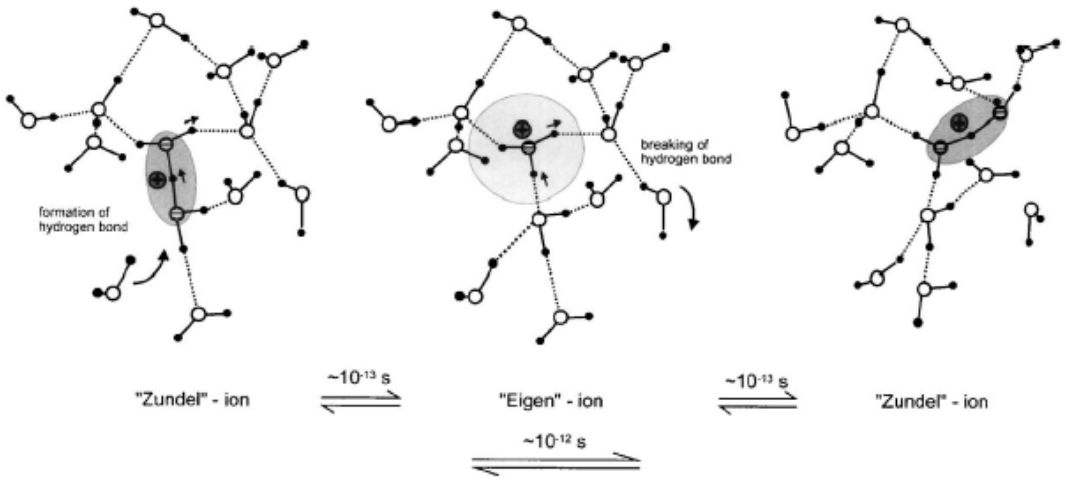


Figure 1.4: Zundel and Eigen Ions [14].

protons, they are all interchangeable, allowing for fast proton transport [16].

Bulk water can be seen as the upper limit of protonic conductivity, and when aqueous systems interact with some environment it serves to decrease that level of conductivity [17]. Therefore, a critical factor in determining the protonic conductivity of a PEM fuel cell is the distribution of the aqueous phase within the ionomer. Figure 1.5 shows a plot of conductivity against water content [18]. One can immediately notice that there is a very steep gradient in the curve as the membrane takes on water. At high water contents, the protonic conductivity in Nafion is very high. It is therefore thought that a well-connected hydrophilic domain of bulk-like water exists within the membrane which carries the majority of the water and proton transport [14]. Water that is close to the sulfonate groups is polarized towards the anion and has much smaller protonic mobility due to the strong electrostatic attraction to the $SO_3^-$ group [14]. It is apparent that determining the morphology of a Nafion membrane, in particular the distribution of water upon hydration, is key to understanding the mobility of protons and hence determining an accurate model for proton and water transport

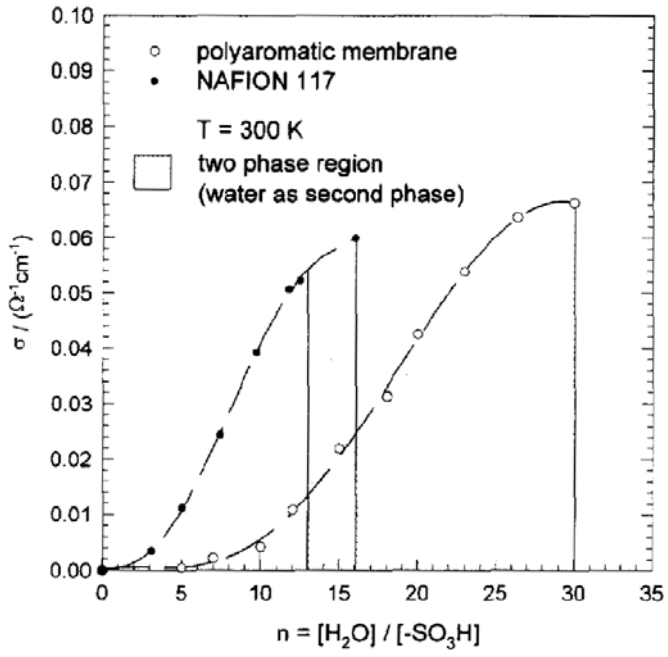


Figure 1.5: Conductivity vs Water Content [18].

## 1.4 Nafion Morphology

Despite intense focus from the academic community and a wealth of experimental data in the literature a 'universally accepted morphological model for the solid-state structure of Nafion has yet to be defined' [6]. The difficulty in establishing a morphological model stems from the random chemical structure of Nafion and the fact that the membrane has structural details which span a wide variety of length scales. Here we highlight some important experimental analyses and morphological models in order to frame the importance of the thermodynamic analysis presented in later sections. For further reading we suggest the review by Heitner-Wirguin [19], and the recent review by Mauritz and Moore [6].

In some of the earliest studies, Gierke et al. examined Nafion with small angle X-ray spectroscopy (SAXS) and wide-angle X-ray diffraction (WAXD) [20], [21],[3]. They found a scattering maximum at small angles which increased in intesity with the specific weight of the

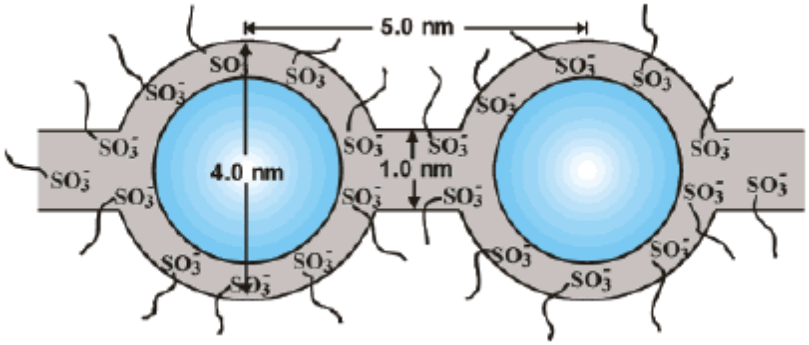


Figure 1.6: Cluster-network model [6].

membrane which they took this as evidence of some crystalline organization within the fluorocarbon matrix. They also observed a scattering peak at angles yielding a Bragg spacing[1] of 3-5 nm, this 'ionomer peak' was found to shift to lower angles and increase in intensity upon further hydration; therefore, Gierke et. al. concluded that it was due to regions high in sulfonate sites that would agglomerate with water (ionic clusters). They postulated these ionic clusters to be spherical inverse micellar in structure. In order to explain the high ionic conductivity found in Nafion, Gierke et al. proposed these clusters were connected by channels yielding a cluster network (see Figure 1.6).

Gierke et al. then estimated the size of the clusters by the amount of water sorbed by the membrane, under the assumption that the clusters were distributed in a cubic lattice configuration. They calculated the diameters to range between 30-50 Å.

Hsu and Gierke presented a model for the hydration and swelling of an ionic cluster [21], [3]. They proposed that the swelling of the membrane can be modeled as the stretching of a continuous medium with a tensile modulus as a function of water content. Their thermodynamic

[1] Bragg spacing (or d spacing) refers to the spacing between scattering 'planes'; in a crystalline object it refers to the distance between planes in the atomic lattice. Constructive interference forms a scattering peak which indicates the d spacing by Bragg's law.

treatment includes contributions to the free energy of the system from the elastic energy of the backbone, interactions between the sulfonate groups and the backbone, the sulfonate groups with each other, and the interactions of three distinct layers of water: water hydrating the sulfonate groups, bulk water, and a layer in between. These interactions are linear in mole number and quantified by interaction parameters.

Weber and Newman refer to the pathways between clusters in Hsu and Gierke's model as 'collapsed channels' [22]. They coin this term because they believe the channel can be expanded and filled by liquid water. In Weber and Newman's model, the channels are regions of the membrane having a low enough concentration of sulfonate heads as to remain hydrophobic. These collapsed channels are assumed to be continuously forming and deforming in ambient conditions due to the movement of free sulfonic acid sites and polymer in the matrix between clusters.

Ioselevich et al. in a recent work suggest a detailed structural model for Nafion-type membrane [23]. In their analysis they assume the micelle-channel model of Gierke and give arguments as to how that structure might be formed by the polymer chains. They argue that Nafion polymer chains attract each other to form bundles, and these bundles form cage-like structures within the membranes. These cages are ion rich and as the membrane sorbs water from a dry state, the cages accommodate the water, forming micellae. At higher water contents these cages are connected by water channels, however. Since there are no jumps in the conductivity curve of Nafion with increasing water content, the formation of channels must not all occur simultaneously; this implies a heterogeneity in the structures. They argue that these channels control the proton conductance; however, there is very little information available on the formation of these necks. Despite this, Ioselevich et al. insist the channels are required to explain the high protonic conductivity of Nafion as in the Gierke model. They outline a methodology in which the formation of channels may be investigated using the minimization of free energy which is a

similar strategy to the analysis employed in this work.

Due to its simplicity, the cluster-network model has served as the foundation of the vast majority of interpretations of experimental data, and for models of the transport phenomena; nevertheless, alternative morphologies have been presented which are also consistent with small angle scattering (SAS) results. An example of the limited nature of SAS results is given by the disagreement on whether the Bragg peak is indicative of interparticle scattering or intraparticle scattering. Due to the complex nature of Nafion, SAS and WAXD studies reveal little morphological detail; therefore, a number of alternative descriptions of Nafion morphology differ significantly in their proposed spatial distribution of ionic domains [6].

A core-shell model was proposed by Fujimura, similar to the Gierke model, where an ion rich core is surrounded by an ion poor shell which are dispersed in a matrix of fluorocarbon chains [24], [25].

Another early model, by Yeager and Steck, proposed the existence of three distinct regions within the membrane: (A) a hydrophobic matrix, (B) an interfacial zone and, (C) ionic clusters [26]. They propose that the ionic clusters are regions within the membrane with a higher concentration of sulfonate acid sites at which the water will tend to agglomerate.

Litt found that SAXS data showed $d$ spacings proportional to the volume of absorbed water in Nafion. From this result he drew the conclusion that ionic domains are hydrophilic layers separated by thin lamellar PTFE crystallites [27]. Upon sorption water separates the PTFE layers yielding a volume growth that is proportional to $d$ spacing. This model leads to parallel shifts of the ionic domain and the crystalline domain. Mauritz notes that in SAS data, the small peak thought to represent the crystalline domain has a dissimilar shift upon sorption than the ionic peak and therefore concludes that this model is likely an oversimplification [6].

Haubold et al. proposed a similar structure to that of Litt, where the side chains and sulfonate

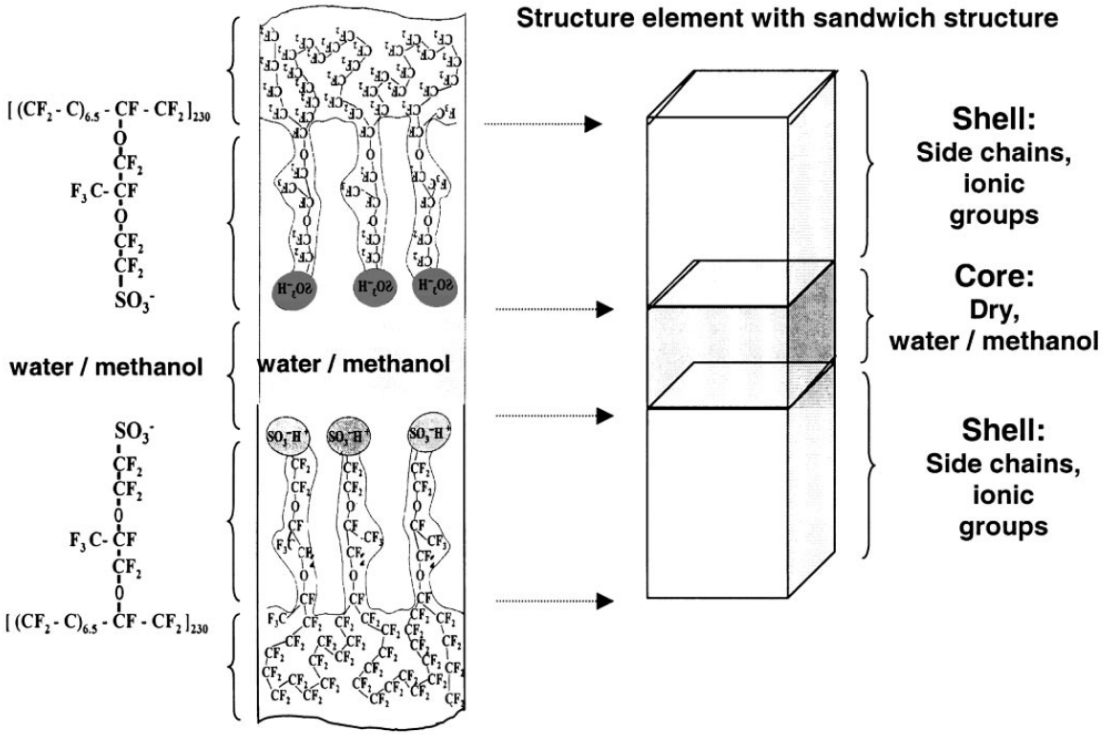


Figure 1.7: Sandwich Structure [28].

groups form shell layers which bound a core layer that can be either dry or filled with solvent, forming a 'sandwich' structure (see Figure 1.7) [28]. These liquid regions interconnect to provide continuous pathways for proton conduction. The core layer and the two shells are estimated to have a total cross section of approximately 6 nm.

A local order model was introduced by Dreyfus et al. which is based on the existence of a short range order, long range gas-like disorder and a fixed number of neighbouring ionic aggregates [29]. In this model the scattering maximum is due to the presence of four first neighbours leading to a diamond lattice structure. Gebel and Lambard found that the local order model produces a better fit to SAS data than does the Fujimura depleted zone shell-core model [30]; however, the local order model has numerous fitted parameters.

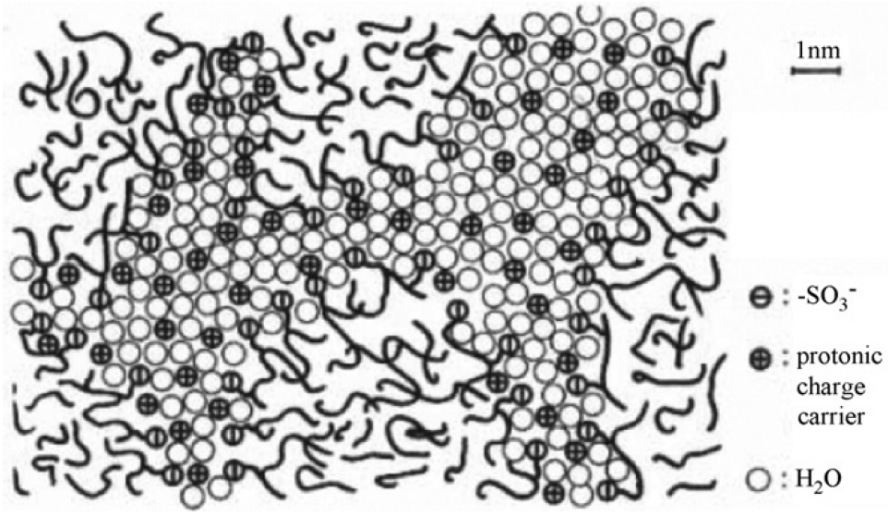


Figure 1.8: Microstructure of Nafion according to Kreuer [31].

In solutions of Nafion (dissolution is achieved at high temperatures) the mixture appears as a colloidal dispersion of rod-like particles. In a model of the structural evolution of Nafion from dry membrane to solution Gebel proposed a dry membrane has isolated spherical ionic clusters [4]. Upon absorption of water these clusters swell, at a volume fraction of water of 0.3 percolation occurs between the clusters, leading to a cluster-network. At a volume fraction of 0.5, a structural inversion is postulated to occur where the polymer is seen as the interconnected network in water and this network goes on to become dispersed in the solvent at higher volume fractions. Mauritz notes that no thermodynamic justification is given for the inversion and that scattering profiles near the inversion point do not show significant change [6].

Kreuer provided an interpretation of SAXS data which is based on the idea of a random arrangement of low dimensional polymeric objects with spaces which can be filled by water (See Figure 1.8) [31]. Kreuer referred to the hydrated region of a Nafion membrane as "well-connected, even at low degrees of hydration i.e., there are almost no dead-end pockets and very good percolation"[32]. Kreuer finds that the water distribution forms continuous pathways throughout the membrane. The permeation of the liquid phase explains the high conductivity of Nafion

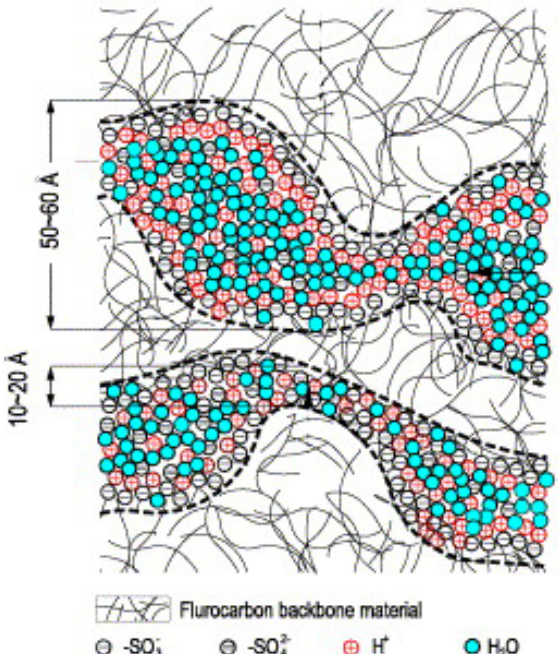


Figure 1.9: Cluster Network Model according to Karimi and Li [33].

and other transport features such as the high electroosmotic drag. Kreuer states that SAXS data alone cannot resolve whether a morphological model such as the cluster-network model is more appropriate. One can see how the cluster-network model can be obtained by simplifying the Kreurer representation, where narrow regions are channels and wide pores are seen as clusters as shown in Figure 1.9 [33].

A number of other methods have been used to investigate the morphology of Nafion membranes in an attempt to contrast the information obtained by SAS techniques. Using a thermodynamic method of standard porosimetry (SPM), Divisek et al. investigated the capillary porous and sorption properties of Nafion membranes [34]. They found that the membranes contain a connected system of pores of a wide range of sizes. They detected pore sizes from 1-100 nm, however the average pore size was found to be 2 nm and the dominant contribution of volume is from the very smallest pores.

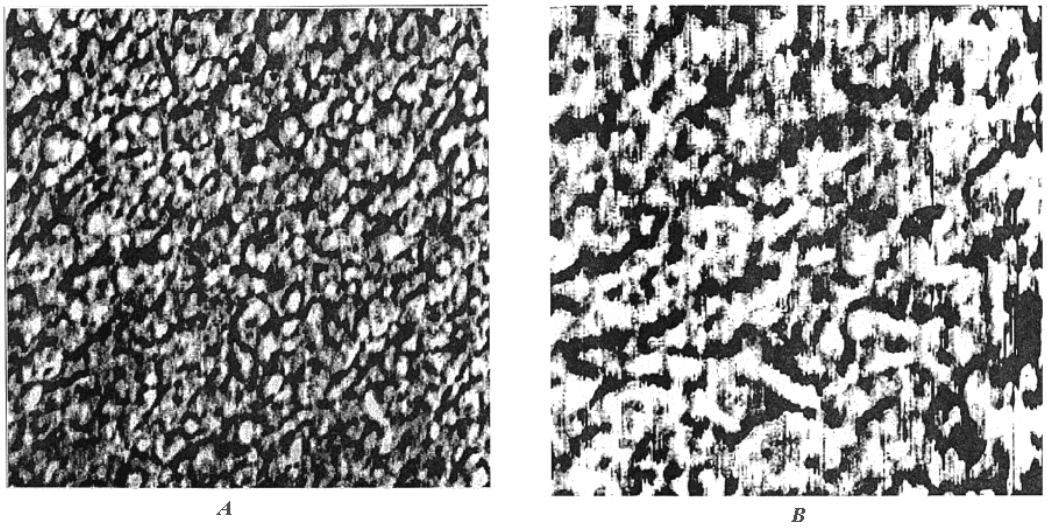


Figure 1.10: AFM Imaging of Nafion [36].

Blake et al. conducted molecular dynamics (MD) simulations to investigate the structure of hydrated $Na^+$ Nafion [35]. They find that at very low water contents (5 wt %) water forms small droplets of size 5-8 Å. Upon hydration the $Na^+$ is dissociated and a percolating hydrophilic network forms. The water forms irregular curvilinear channels of cross section 10-20 Å which branch in all directions. Due to the small cross section, the ion concentration in the channels was found to be quite high. Blake et al. also note that the side chains tend to line up along the channel walls with the $SO_3^-$ sticking out into the hydrophilic domain, in an effort to minimize the surface free energy.

McLean et al. investigated $K^+$ form Nafion membranes using Atomic Force Microscopy (AFM). AFM involves developing an image which contrasts surface or near surface elasticity [36]. In tapping mode the AFM probe undergoes low energy oscillations incident to the membrane surface. The soft regions are deemed regions which contain ionic groups at or near the surface whereas fluorocarbon backbone is purported to be the harder regions. The results of the AFM imaging in tapping mode are shown in Figure 1.10. The images show 300 nm × 300 nm sections

of Nafion 117. The ionic species are shown in light regions whereas the darker regions represent stiffer backbone. Figure 1.10 A is from the membrane exposed to ambient conditions. We find ionic 'clumps' with sizes which range from 4-10 nm. However in Figure 1.10 B, which shows the membrane in contact with saturated liquid, we see that the clump sizes have grown to 7-15 nm and the ionic regions appear to form continuous channels which would provide pathways for proton conduction. It is interesting to note that we see no long range pattern of clusters in the AFM imaging and in fact the well hydrated image is very similar to the representation put forward by Kreuer discussed earlier. It is important to note that, while this imaging was done on the neutral $K^+$ form Nafion, Gebel and Lambard show that neutral forms of Nafion seem to have extremely similar SAS profiles upon sorption [30].

As we noted earlier, information on the morphology of Nafion yields insight important for formulating consistent transport models for protons and water through the membrane. Eikerling et al. presented a theory for transport based on the cluster-network model [5]. In their model, clusters and channels are connected at random. Furthermore they postulated that there are two different types of clusters and channels (which we call pores): those which fill with bulk water and swell upon sorption and those that contain only surface water (i.e., water strongly bound to sulfonate sites in upon dissociation), which do not swell with bulk water and retain their original shape. The pores containing bulk water have a much higher conductivity than those without. In Figure 1.11 A we see an illustration of the network of filled and unfilled pores, and in Figure 1.11 B we see a representation of the surface of a filled pore. Although their model does not include an analysis on which pore fills, Eikerling et al. note that the equilibrium size of the water filled pore is a balance between elastic and osmotic forces and go on to stipulate that determining the factors governing swelling of pores is an important step in the optimizing of membrane design.

In an analysis [37] on Schroeder's paradox [9] and subsequent work on membrane sorption and

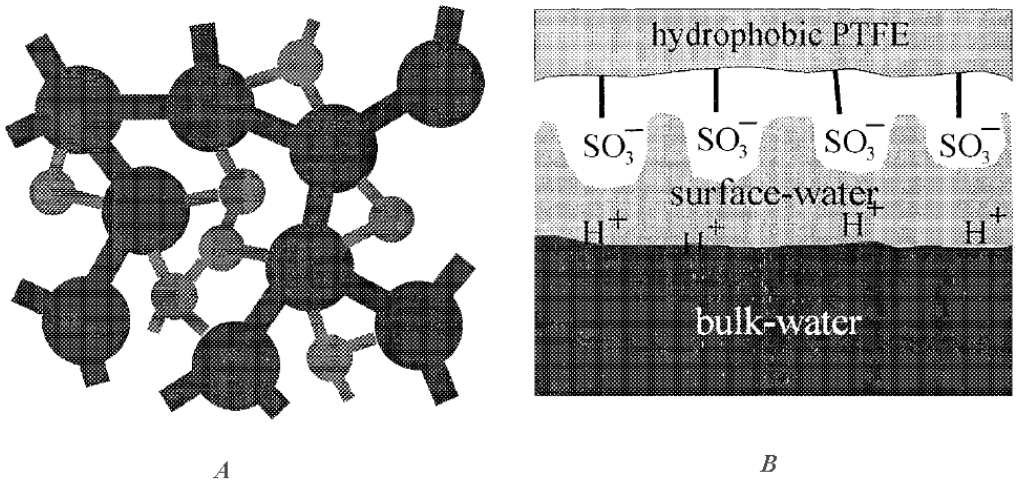


Figure 1.11: Eikerling 2-pore model [5].

transport [38] [15], Choi et al. model the membrane as a series of pores of equal radius. In Figure 1.12 we see the pore structure for the transport model. In their model, when the water content is low, the hydrophilic phase is small, with a low enough water content not all acid sites are dissociated [15]. With less water molecules, there is a decreased level of interaction of water through hydrogen bonding, and this therefore leads to a higher energy requirement to break bonds and a lowered dielectric constant [15]. There is therefore at low levels of water content a low rate of proton transfer, which is primarily limited to the surface region through a proton. To describe sorption of the Nafion membrane Choi et al. incorporate a model for water uptake proposed by Futerko and Hsing using Flory-Huggins theory which fits sorption isotherms to the Flory-Huggins equation by means of the Flory interaction parameter [39].

In another model using the cylindrical pore approach Paddison et al. [40] focus on water filled cylindrical pores of variable $L$ and $r$, and they state that it is critical to determine the water-containing phase as it is the region through which conduction occurs.

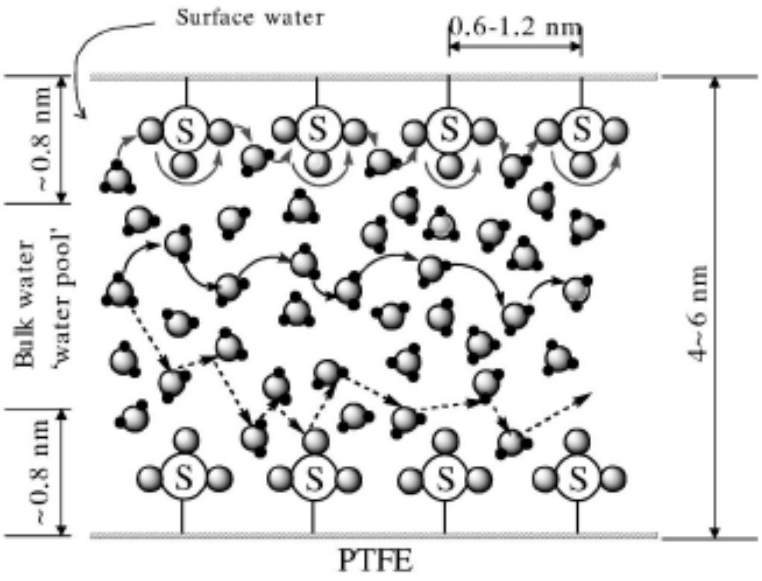


Figure 1.12: Bulk and Surface Water in a Pore [15].

## 1.5 Objectives of this Work

Since the transport through bulk water presents an upper limit for protonic conductivity, it is important to determine the permeation of the liquid phase and its connectivity in order to quantify the various modes of proton transport. The morphological models presented in the previous section are wide ranging. We tend to favour the interpretation of Kreuer [31], which is reflected in the AFM imaging conducted by McLean et al.[36]; however, it is easy to see that the morphological models which present more order, such as the cluster network model or the 'sandwich' structured model are merely distillations of such an interpretation.

In this work, along with the work in [41], we aim at adding analytical insight to the wealth of experimental work done in determining the morphology of Nafion. Previous work such as that done by Choi et al.[37] [38], and Futerko and Hsing [39], determine sorption in the membrane as a whole in order to quantify sorption isotherms. The present work focuses on the sorption on the scale of micropores [34], in order to help quantify the complex microstructure of Nafion as

it sorbs water, in particular the distribution and connectivity of the hydrophilic domain which dramatically impacts the protonic conductivity. We noted earlier that geometric conditions affect the stability of liquid water in hydrophobic confines and we shall examine in particular the stability of water in a single microscopic pore by means of a parametric analysis of the wettability of a Nafion micropore. In other words, this paper aims to determine in which regions of a Nafion membrane water would be stable in the liquid phase, in order to give insight on the permeation of the liquid phase. In the context of the work of Eikerling et al. we determine the factors which determine which pores are liquid filled, and those which contain only surface water.

Kreuer suggests that the different regions within a Nafion membrane do not conform to geometric ideals; however, in this work we simplify the structure much the same as in the cluster-network model. We model regions in the Nafion membrane as spherical pores of water such as those introduced by Hsu and Gierke [3], and cylindrical shaped pores (or channels).

As is done by Hsu and Gierke in [3], the relevant thermodynamic forces contributing to the total free energy are modeled. For a cylindrical pore (or channel) we shall compute and plot the free energy of the pore filled with liquid of length $L$ against a vapor filled reference state. We determine which state is stable for a given pore radius $r_0$. We find a critical radius $r_c$ for which liquid is never stable, and show that there exists a critical liquid length $L_{crit}(r)$ for all pore radii larger than $r_c$. For pores that fill with liquid we show how swelling occur and how. the increase in free energy due to swelling leads to a minimum of the free energy of the system. For the spherical pore the results are compared to those proposed by Hsu and Gierke [3].

In this work we specify, under the given assumptions, the thermodynamic conditions necessary for the sorption and swelling of water in Nafion pores. If this work is coupled with a sufficiently flexible pore size distribution model, a complete picture of water connectivity within the membrane can be established. These results also help form some intuition regarding the SAXS

experimental results prevalent in the literature. We also discuss how this model accounts for a difference in uptake between saturated liquid and saturated vapor equilibrated membranes, and gives support to Weber and Newman's [22] notion that some channels fill or collapse depending on the phase at the boundary.

# Chapter 2

# Thermodynamics of Sorption

## 2.1 System

In order to detail the thermodynamic forces which govern the equilibrium state of water in Nafion, a section of a Nafion membrane is considered in a closed system with a given pressure $p$ and temperature $T$, such as one might find in an experimental apparatus. The system is considered large in comparison to the size of the membrane such that liquid condensing into the membrane represents an insignificant mass fraction of the total water in the system. Two scenarios are modeled: a cylindrical pore open at both ends to the environment (see Figure 2.1) which may fill with liquid water, and a spherical pore within the Nafion membrane (see Figure 2.2).

As discussed further in this section, the environment considered is at or near saturation and therefore the chemical reaction dissociating the sulfonate sites is considered to have occurred, whether or not bulk-like liquid fills the pore. Also, while water is considered here, this analysis should be equally applicable to similar solvent systems as the unique aspects of water protonation discussed in the introduction do not feature in this analysis. This is reasonable because, as discussed earlier, experimental results on the sorption of neutral form Nafion shows little difference to the standard acidic form

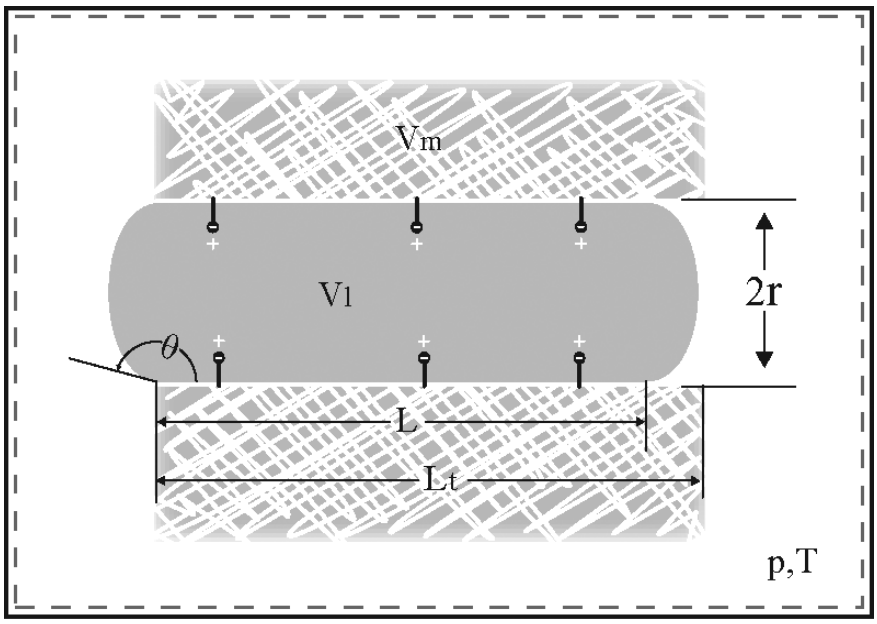


Figure 2.1: Cylindrical Pore System.

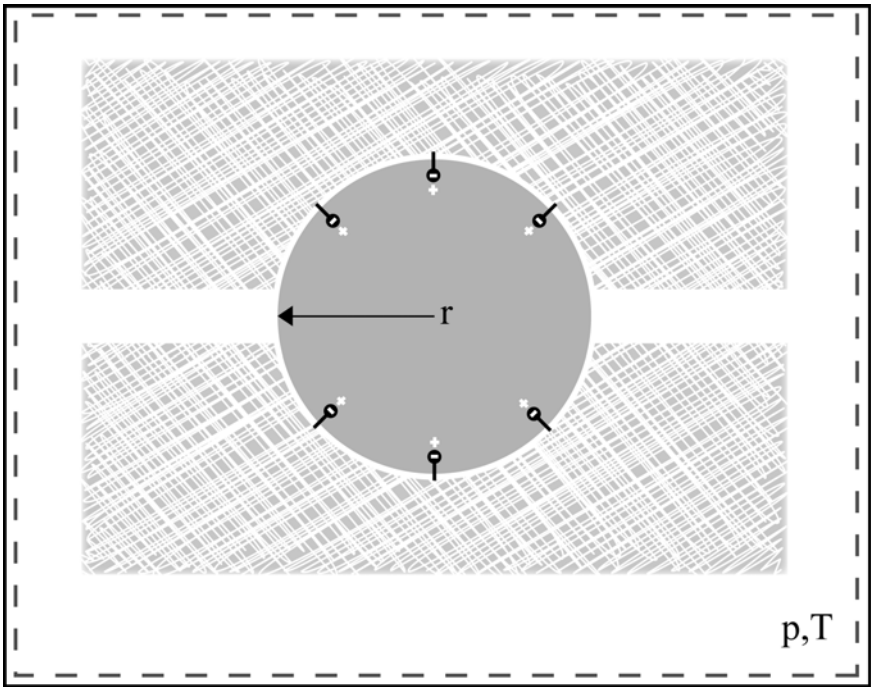


Figure 2.2: Spherical Pore System.

### 2.1.1 Cylindrical Pores

In the analysis of liquid stability in a cylindrical pore it is assumed that the liquid agglomeration fills the pore radially and the filling length $L$ is varied to determine stable configurations, or the pore is assumed empty. Situations in which the radius of the liquid $r$ is smaller than the unswollen radius of the pore $r_0$ are not considered.

The surface area of liquid in the pore, $A_l$, is composed of the area of the cylindrical portion $A_c$ and the area of the ends $A_{end}$,

$$A_l = A_c + 2A_{end}\,. \tag{2.1}$$

$A_l$ is a function of radius $r$, length $L$ and contact angle $\theta$,

$$A_l = 2\pi rL + 2\pi r^2 a_\theta \tag{2.2}$$

where

$$a_\theta = \frac{2}{1+\sin\theta}\,. \tag{2.3}$$

Likewise, the volume of liquid in the pore, $V_l$, is comprised of the volume of the cylindrical region $V_c$ and the volume in the curved ends, $V_{end}$,

$$V_l = V_c + 2V_{end}\,. \tag{2.4}$$

The explicit expression is

$$V_l = \pi r^2 L + 2\frac{\pi}{3}r^3 b_\theta \tag{2.5}$$

where

$$b_\theta = 2\sec^3\theta\,[\sin\theta - 1] + \tan\theta\,. \tag{2.6}$$

It is important to note that in this description, even when the length $L$ of the liquid agglomeration is zero, $V_l$ refers to a 'lentil' of volume $2V_{end}$, due to the curved ends. The derivation of $a_\theta$, and $b_\theta$ is given in Appendix A.

### 2.1.2 Spherical Pores

As with the cylindrical pores, the spherical agglomerations are considered to fill the region they are in, however the collection of water is permitted to have fractional contact with the backbone. As shown in Figure 2.2, the spherical agglomeration of liquid water has partial contact with the Nafion backbone and a liquid-vapor interface where connected to channels. We introduce a constant $n$, such that the area of the solid-liquid interface is $nA_l$ and the area of the liquid-vapor interface is then $(1-n)\,A_l$. We assume that contact with the backbone does not alter the shape of the agglomeration from that of a perfect sphere in order to keep the mathematics reasonable. The area of the liquid is therefore given simply by

$$A_l = 4\pi r^2 \tag{2.7}$$

and the volume is given by

$$V_l = \frac{4}{3}\pi r^3. \tag{2.8}$$

## 2.2 Nature of Equilibrium

From the first and second laws of thermodynamics, for a system with fixed external pressure and temperature, one finds

$$\frac{d\mathcal{G}}{dt} \leq 0 \tag{2.9}$$

where $\mathcal{G} = F + pV$ is the total free energy (sometimes also referred to as available free energy [42]) of the system. Equation (2.9) states that the total free energy of the system decreases in time, such that $\mathcal{G}$ assumes a minimum in equilibrium. All contributions to the free energy must be included in order to determine equilibrium conditions. A formal approach is followed here as laid out by laid out by Müller in his classic treatise on thermodynamics [43], this approach is also used by Morro and Müller [44], and by Bensberg [45], for the case of polyelectrolyte gels. Writing out all contributions to $\mathcal{G}$ in terms of the Helmholtz free energy in the unmixed state, $F_\alpha = f_\alpha(v)m_\alpha$, and the Gibbs free energy of mixing, $G_{\alpha,mix}$, gives

$$\mathcal{G} = F_l + G_{l,mix} + F_p + G_{p,mix} + F_v + F_s + F_m + p\left(V_l + V_p + V_v + V_m\right) . \tag{2.10}$$

The subscripts $\alpha = l$, $p$, $v$, $s$, and $m$ refer to the liquid, protons, vapor, surface and membrane, respectively. Since the membrane is phase-separated there is no mixing of the polymer chains with the liquid in the pore and thus no corresponding entropic contributions.

Equation (2.10) is our governing equation in its most general form. We now transform this equation through constitutive relations and mathematical techniques along with various assumptions into a function of variables (namely those which define the geometry of the system) we are concerned with.

With the free energy of mixing given explicitly, (2.10) yields

$$\begin{aligned}\mathcal{G} = \left[f_l + R_l T \ln a_l\right] m_l + \left[f_p + R_p T \ln a_p\right] m_p + f_p^0 m_p^0 \\ + f_v m_v + F_s + F_m + p\left(V_l + V_p + V_p^0 + V_v + V_m\right) .\end{aligned} \tag{2.11}$$

Here, $R$ denotes the gas constant. The protons within the liquid mixture are referred to by $m_p$ and $V_p$ while the protons outside the liquid boundary are denoted by $m_p^0$ and $V_p^0$. The total

mass of protons in the pore

$$m_p^T = m_p + m_p^0, \tag{2.12}$$

is constant. Under the assumption that the protons are incompressible, the total volume of the protons stays constant. The activity $a_\alpha$ is defined as

$$a_\alpha = \gamma_\alpha^a X_\alpha \tag{2.13}$$

where $\gamma_\alpha^a$ is the activity coefficient and $X_\alpha$ is the mole fraction in the mixture. The mole fraction of the liquid water in the mixture is given by

$$X_l = \frac{N_l}{N_l + N_p}\,, \tag{2.14}$$

and the mole fraction of the protons in the mixture $X_p = 1 - X_l$.

By means of (2.13) the free energy of the system can be rewritten as

$$\begin{aligned}\mathcal{G} = {} & \left[f_l + R_l T \ln X_l\right] m_l + \left[f_p + R_p T \ln X_p\right] m_p + f_p^0 m_p^0 \\ & + f_v m_v + F_s + F_m + p\left(V_l + V_p + V_p^0 + V_v + V_m\right) + R_u T\left(N_l \ln \gamma_l^a + N_p \ln \gamma_p^a\right). \end{aligned} \tag{2.15}$$

The last term represents the excess Gibbs free energy of mixing $G_{mix}^E$, that is the energy difference with respect to ideal mixing. This can be expressed in terms of a Flory interaction parameter $\chi_{\alpha\beta}$ [46], as

$$\frac{G_{mix}^E}{R_u T} = \left(N_l \ln \gamma_l^a + N_p \ln \gamma_p^a\right) = N_p X_l \chi_{pl}\left(T\right). \tag{2.16}$$

With (2.16), Equation (2.15) can be written as

$$\mathcal{G} = [f_l + R_l T \ln X_l]\, m_l + [f_p + R_p T \ln X_p]\, m_p + f_p^0 m_p^0 + f_v m_v + F_s + F_m + p\left(V_l + V_p + V_p^0 + V_v + V_m\right) + R_u T N_p X_l \chi_{pl}. \quad (2.17)$$

To determine equilibrium states, we must minimize the total free energy $\mathcal{G}$ with respect to those variables that will change in time as equilibrium is approached: the mass of liquid in the pore $m_l$, the mass of vapor $m_v$, the volume of vapor $V_v$, and the volume of liquid $V_l$. Since we are considering a closed system, the total mass stays constant,

$$m_w = m_l + m_v = const\,. \quad (2.18)$$

Hence, the conditions for equilibrium are

$$\frac{\partial \mathcal{G}}{\partial m_l} = \frac{\partial \mathcal{G}}{\partial V_l} = \frac{\partial \mathcal{G}}{\partial V_v} = 0\,. \quad (2.19)$$

The details of setting each derivative equal to zero reveal further information about equilibrium states.

Minimizing the total free energy with respect to the mass of liquid, $m_l$, yields

$$\frac{\partial \mathcal{G}}{\partial m_l} = f_l + R_l T \ln X_l + m_l \frac{\partial f_l}{\partial v_l}\frac{\partial v_l}{\partial m_l} + m_l R_l T \frac{\partial \ln X_l}{\partial m_l} + m_p R_p T \frac{\partial \ln X_p}{\partial m_l} - f_v - m_v \frac{\partial f_v}{\partial v_v}\frac{\partial v_v}{\partial m_v} + m_p R_p T \chi_{pl}\frac{\partial X_l}{\partial m_l} = 0\,. \quad (2.20)$$

With the Gibbs-Duhem relation [47],

$$m_l R_l T \frac{\partial \ln a_l}{\partial m_l} + m_p R_p T \frac{\partial \ln a_p}{\partial m_l} = 0 \quad (2.21)$$

and the Maxwell relation [47],

$$\left(\frac{\partial f_\alpha}{\partial v_\alpha}\right)_{t=const.} = -p_\alpha \tag{2.22}$$

this simplifies to

$$\frac{\partial \mathcal{G}}{\partial m_l} = f_l + R_l T\left(\ln X_l + \chi_{pl} X_p^2\right) + p_l v_l - f_v - p_v m_v = 0\,. \tag{2.23}$$

where $p_l$ represents the pressure of the mixture $p_{mix}$. Using the relation between free energies

$$g_\alpha = f_\alpha + p_\alpha v_\alpha \tag{2.24}$$

(2.23) can be rewritten as

$$g_l + R_l T \ln a_l = g_v \tag{2.25}$$

Equation (2.25) states the classical result that the chemical potentials of the liquid and vapor are equal in equilibrium.

Minimizing the total free energy with respect to the volume of the vapor yields

$$\frac{\partial \mathcal{G}}{\partial V_v} = m_v \frac{\partial f_v}{\partial v_v}\frac{\partial v_v}{\partial V_v} + p = 0\,. \tag{2.26}$$

This reduces to

$$-p_v + p = 0 \tag{2.27}$$

which means that the pressure of the vapor is equal to the external pressure imposed on the system.

Minimizing the total Gibbs free energy with respect to the volume of the liquid gives

$$\frac{\partial \mathcal{G}}{\partial V_l} = m_l \frac{\partial f_l}{\partial v_l}\frac{\partial v_l}{\partial V_l} + m_l R_l T \frac{\partial \ln X_l}{\partial V_l} + m_p R_p T \frac{\partial \ln X_p}{\partial V_l} + f_p \frac{\partial m_p}{\partial V_l} + R_p T \ln X_p \frac{\partial m_p}{\partial V_l} + f_p^0 \frac{\partial m_p^0}{\partial V_l} + p + \frac{\partial F_s}{\partial V_l} + \frac{\partial F_m}{\partial V_l} + R_p T \chi_{pl} \left[ X_l \frac{\partial m_p}{\partial V_l} + m_p \frac{\partial X_l}{\partial V_l} \right] = 0 \,. \quad (2.28)$$

Simplifying this with (2.12) and the Gibbs-Duhem relation leads to

$$\frac{\partial \mathcal{G}}{\partial V_l} = \frac{\partial f_l}{\partial v_l} + \left[ f_p - f_p^0 + R_p T \left( \ln X_p + \chi_{pl} X_l^2 \right) \right] \frac{\partial m_p}{\partial V_l} + p + \frac{\partial F_s}{\partial V_l} + \frac{\partial F_m}{\partial V_l} = 0 \,. \quad (2.29)$$

We define the surface pressure,

$$p_s = \frac{\partial F_s}{\partial V_l} \,, \quad (2.30)$$

which is due to the change in surface free energy with the liquid volume, and the membrane pressure,

$$p_m = \frac{\partial F_m}{\partial V_l} \,, \quad (2.31)$$

which is due to the change of membrane free energy with liquid volume. We also define a proton pressure

$$p_p = \left[ f_p - f_p^0 + R_p T \left( \ln X_p + \chi_{pl} X_l^2 \right) \right] \frac{\partial m_p}{\partial V_l} = \left[ f_p - f_p^0 + R_p T \ln a_p \right] \frac{\partial m_p}{\partial V_l} \quad (2.32)$$

which is related to the energy required to add more protons to the mixture as the boundary of $V_l$ expands. We can thus rewrite (2.29) as

$$p_{mix} = p + p_s + p_m + p_p \quad (2.33)$$

which states that the pressure of the liquid/proton mixture is a function of the energies of the surface, membrane, and protons in the mixture.

We can also, of course, consider the liquid to be incompressible a priori and we can therefore couple two of these variables by means of $m_l = \rho V_l$. The results are naturally identical to the above; details are given in Appendix B.

We now can substitute the pressure of the mixture (2.33) into the total free energy (2.11), replace the specific Helmholtz free energy $f$ with the Gibbs free energy $g$, and use (2.18) to find

$$\begin{aligned}\mathcal{G} = \left[g_l + R_l T \ln X_l\right] m_l + \left[g_p + R_p T \ln\left(X_p + \chi_{pl} X_l\right)\right] m_p + g_p^0 m_p^0 \\ + g_v m_w - g_v m_l + F_m + p V_m - \left(p_s + p_m + p_p\right)\left(V_l + V_p\right) + F_s \,. \quad (2.34)\end{aligned}$$

Since we take vapor as an ideal gas we have

$$g_v\left(p_v\right) = g_v\left(p_{sat}\right) + R_v T \ln\left(\frac{p}{p_{sat}}\right) = g_l\left(p_{sat}\right) + R_v T \ln\left(\frac{p}{p_{sat}}\right) \quad (2.35)$$

where we used the equilibrium relation

$$g_v\left(p_{sat}\right) = g_l\left(p_{sat}\right).$$

We can approximate the Gibbs free energy at saturation by performing a Taylor series expansion about our reference pressure

$$g_l\left(p_{sat}\right) = g_l\left(p\right) + \frac{\partial g_l}{\partial p}\left(p_{sat} - p\right) + \frac{1}{2}\frac{\partial^2 g_l}{\partial p^2}\left(p_{sat} - p\right)^2 + ... \quad (2.36)$$

Since we assume water is incompressible, all second order and higher terms vanish, and the approximation becomes exact. Using the Maxwell relation

$$\left(\frac{\partial g_\alpha}{\partial p_\alpha}\right)_{t=const.} = v_\alpha \quad (2.37)$$

with (2.36), (2.35) becomes

$$g_v(p_v) = g_l\,(p) + (p_{sat} - p)v_l + R_v T \ln\left(\frac{p}{p_{sat}}\right). \tag{2.38}$$

We use a similar Taylor expansion to arrive at

$$g_l(p_{mix}) = g_l(p + p_s + p_m + p_p) = g_l(p) + v_l\,(p_s + p_m + p_p)\ . \tag{2.39}$$

We also assume that the protons are incompressible so that

$$g_p\,(p_{mix}) = g_p + v_p\,(p_s + p_m + p_p)\,. \tag{2.40}$$

We then substitute (2.38), (2.39) and (2.40) into the total free energy (2.34) with $p_r = p/p_{sat}$, $R_l = R_v = R_w$, and $X_p = 1 - X_l$, to obtain

$$\begin{aligned}\mathcal{G} = \left[(p - p_{sat}) + \frac{R_w T}{v_l}\ln\left(\frac{X_l}{p_r}\right)\right] V_l \\ + \left[g_p\,(p) + R_p T\left(\ln(1 - X_l) + \chi_{pl} X_l\right)\right] m_p \\ + g_p^0 m_p^0 + g_v m_w + F_m + pV_m + F_s\,.\end{aligned} \tag{2.41}$$

We see that the pressure within the pore $p_{mix}$ is no longer explicit.

We introduce as a reference state, the free energy of a vapor filled pore

$$\mathcal{G}^0 = g_v m_w + g_p^0\,(p)\, m_p^T + F_m^0 + pV_m^0 + F_s^0\,. \tag{2.42}$$

Subtracting this reference from (2.41) gives

$$\mathcal{G} - \mathcal{G}^0 = \left[(p - p_{sat}) + \frac{R_w T}{v_l} \ln\left(\frac{X_l}{p_r}\right)\right] V_l + \left[g_p(p) - g_p^0(p) + R_p T\left(\ln(1 - X_l) + \chi_{pl} X_l\right)\right] m_p + F_m - F_m^0 + p\left(V_m - V_m^0\right) + F_s - F_s^0. \quad (2.43)$$

We are interested in determining whether liquid or vapor is energetically favorable in a given pore. By subtracting the free energy of a vapor filled pore, we know that if the difference $\mathcal{G} - \mathcal{G}^0$ is negative, then the free energy of the vapor state is lower and therefore the vapor filled state is stable in equilibrium. Subtraction of $\mathcal{G}^0$ also conveniently eliminates various constants if $r = r_0$, which occurs when we do not consider membrane swelling. We still have unknown functions remaining in the free energy of the protons $g_p(p) - g_p^0(p)$, the free energy of the membrane $F_m - F_m^0$, and the free energy of the surfaces $F_s - F_s^0$. The subsequent sections detail revealing the structure of these functions.

### 2.2.1 Dissociation

Initially the $H^+(H_2O)_n$ is very strongly bound to the $-SO_3^-$ group where the proton originated. As more waters are attracted to this acid site, a fraction of the water is strongly bound in proton-transfer complexes [39]. This reduces the effective water content of the membrane, and in turn increases the mobility of the dissociated proton. It was proposed by Futerko et al. to treat the fraction of waters strongly bound to the acid site $\lambda_C$ (akin to chemisorption) as part of the polymer, separate from the water that is free to equilibrate the chemical potential of the system $\lambda_F$ [39]. Therefore the total number of waters per acid site in the membrane is given as $\lambda = \lambda_F + \lambda_C$.

Choi and Datta describe the formation of the hydration shell as a stepwise equilibrium in which

the binding of the solvent molecules in the shell is assumed to occur in $n$ sequential reactions between the polymer acid groups and the polar solvent molecules [37]. The first of those steps is the formation of the hydronium ion and subsequent steps represent further solvation. Choi and Datta delineate that solvent molecules with equilibrium constants $K \leq 1$ may be assumed weakly bound enough to be accounted for in physical equilibrium. This yields the number of strongly bound waters as

$$\lambda_C = \lambda_m \frac{K_1 a}{1-a} \left( \frac{1 - (n+1)\,(a)^n + n\,(a)^{n+1}}{1 + (K_1 - 1)\,a - K_1\,(a)^{n+1}} \right) \tag{2.44}$$

where $K_1$ is the equilibrium constant for the first (and dominant) reaction step, $a$ is the activity of the water, and $\lambda_m$ is an empirical solvation parameter to adjust for the fact that only $K_1$ is used.

A key point in our analysis is that for the vapor filled reference state we assume that the dissociation reaction has taken place and $\lambda_C$ water molecules are strongly bound to the sulfonate site. The number of these waters is evaluated through the law of mass action as described by Choi and Datta. These waters are strongly bound and exist regardless of whether a liquid phase fills the pore. For the purpose of this work, we assume that the subsequent waters which form the liquid phase do not significantly alter the free energy of the protons, therefore the $g_p\,(p) - g_p^0\,(p)$ term is negligible and the bulk-like waters $\lambda_F$ contribute in altering the total free energy due to mixing only.

### 2.2.2 Elastic Free Energy

The change in the free energy of the membrane describes elastic forces and only contributes when the membrane swells to $r > r_0$, to allow more water into the pore. We assume that when the membrane swells, the volume of the membrane backbone itself remains constant, i.e., $V_m = V_m^0$ for all $r$. The change in volume of the system is therefore only due to the increasing

water volume.

The change in free energy of a polymer is entropic. In Nafion, as in rubber [42], when the material is stretched the polymer chains have their configurational entropy reduced. The complexity with Nafion is that water is strongly attracted to the acid sites while the PTFE backbone (Teflon) is hydrophobic which induces a phase separation within the membrane.

A model was constructed by Flory and Rehner for the swelling of a polymer network [46], which assumes random mixing of solvent and monomers, and linear strain in the deformation of the chains comprising the network [8]. The classical Flory-Rehner model also assumes a Gaussian distribution of polymer chain lengths. The Gaussian assumption is only reasonable for chain lengths which are very long, such as in rubber with 400 or more monomers in the chains between cross-links; the Gaussian assumption fails for chain lengths of less than about 100 monomers [48]. Flory [46] finds the change in free energy

$$F_m - F_m^0 = \Delta F_{el} = \frac{kT\nu_e}{2}\left[\alpha_1^2 + \alpha_2^2 + \alpha_3^2 - 3 - \ln\left(\alpha_1\alpha_2\alpha_3\right)\right] \tag{2.45}$$

where $k$ is the Boltzmann constant and $\alpha_\beta$ is the linear deformation factor. $\nu_e$ is the elastically effective number of chains in the polymer network. If crosslinks are present then $\nu_e$ represents the chain segments between crosslinks. We use the effective number of chains because polymers other than Nafion may contain crosslinks; evidence of the effect of crosslinking on sorption in polymide membranes is detailed in [49]. A slight modification of (2.45) is used by Morro and Müller in [44].

Freger points out that for a phase-separated polymer network such as Nafion, the assumption made in Flory-Rehner theory may not be appropriate; that neglecting the interaction of the aggregates upon swelling is too large a simplification [8]. Freger has developed an adaptation of the classical Flory-Rehner model which describes the phase-separated swelling of the hydropho-

bic matrix as an 'inflation' rather than a dilution. Freger proposes [8], for isotropic swelling ($\alpha_\beta = \alpha$), the form

$$\Delta F_{el} = \frac{kT\nu_e}{2V_0}\left[2\alpha^{-2/3} + \alpha^{4/3}\right]. \tag{2.46}$$

In this analysis we use Flory's form, despite the concerns raised by Freger over its accuracy with respect to the complex morphology of Nafion. Since we consider a single microscopic pore, the phase separation is already considered explicitly. Also Freger's form is not used as it would give a nonphysical finite elastic free energy in the undeformed state.

To define the number of chains that a pore is stretching we assume that the volume of membrane being swollen is linearly proportional to the volume of the pore

$$V_m^T = \frac{V_0}{\phi}. \tag{2.47}$$

Here $V_m^T$ refers to the total membrane volume, which includes pore and backbone. The constant $\phi$ is a measure of the porosity of the dry membrane and $V_0$ refers to the volume of the unswollen pore in the membrane. What this means is that each pore stretches a region of the membrane which is proportional to its own volume. This divides the membrane in pores and the volume of membrane that bounds in a strategy similar to that employed by Freger. Therefore the number of chains is assumed to be

$$\nu_e = \frac{V_0 A_v}{\phi \bar{V}_m^T} \tag{2.48}$$

### 2.2.3 Surface Free Energy

The surface free energy is the additional free energy required to remove a molecule from the bulk in order to create an interface between two coexisting phases [50]. This energy is linearly proportional to the surface area of the interface,

$$F_s = \gamma \int dA\,, \tag{2.49}$$

where $\gamma$ is the interfacial tension which has units of energy per unit area. In our system we have three phase interfaces, and thus the surface free energy of the system is

$$F_s = \gamma_{sv} A_{sv} + \gamma_{sl} A_{sl} + \gamma_{lv} A_{lv} \tag{2.50}$$

where $\gamma_{sv}$, $\gamma_{sl}$ and $\gamma_{lv}$ are the interfacial tensions of the solid-vapor, solid-liquid and liquid-vapor interfaces, respectively [50]. We also note that Young's equation [51],

$$\frac{\gamma_{sv} - \gamma_{sl}}{\gamma_{lv}} = \cos\theta\,, \tag{2.51}$$

relates the surface tensions to the contact angle at the three phase point.

### 2.2.4 Chemical Potential

The equality of the chemical potentials of liquid and vapor (2.25) can be used in conjunction with the conditions of mechanical equilibrium (2.27), and (2.33) to indicate the equilibrium of the system, however, in our case this approach lacks sufficient flexibility to observe the effects of pore size change. We can eliminate the unknown Gibbs functions as done previously; using the liquid and vapor pressures and assuming the liquid is incompressible and that the vapor is an ideal gas, we can rewrite (2.25) as

$$g_l\left(p\right) + v_l\left(p_s + p_m + p_p\right) + R_l T \ln X_l = g_v(p_{sat}) + R_v T \ln\left(\frac{p}{p_{sat}}\right)\,. \tag{2.52}$$

With $g_l\left(p_{sat}\right) = g_v(p_{sat})$, we get

$$g_l\left(p\right) + v_l\left(p_s + p_m + p_p\right) + R_l T \ln X_l = g_l(p) + v_l\left(p_{sat} - p\right) + R_v T \ln\left(\frac{p}{p_{sat}}\right) \tag{2.53}$$

or

$$p_{mix} - p_{sat} = \frac{R_w T}{v_l} \ln\left(\frac{p_r}{X_l}\right) . \tag{2.54}$$

The relation requires the evaluation of the pressure of the mixture, $p_{mix}$, which contains terms that are in differential form. We therefore prefer to seek a minimum of total free energy (2.43), rather than evaluating the conditions of its derivatives (2.25) , (2.30), (2.31) and (2.32).

## 2.3 Cylindrical System

We now impose the geometry of the cylindrical pores. The mass of the protons may be expressed through the surface density of sulfonate sites $S_p$ (which are assumed to be ionized) and the surface area of the unswollen pore in contact with liquid $A_c$ as

$$m_p = M_p S_p 2\pi r_0 L \tag{2.55}$$

where $M_p$ is the molar mass.

The surface energy $F_s$ given by (2.50) for a liquid agglomeration of length $L$ in a cylindrical pore of total length $L_t$ becomes

$$F_s = \gamma_{sv} 2\pi r(L_t - L) + \gamma_{sl} 2\pi r L + 2\gamma_{lv}\pi r^2 a_\theta . \tag{2.56}$$

Using Young's equation (2.51) to relate the interfacial tensions to the contact angle with the membrane, (2.56) can be rewritten as

$$F_s = \gamma_{sv} 2\pi r L_t - 2\pi r L \gamma_{lv} \cos\theta + 2\gamma_{lv}\pi r^2 a_\theta . \tag{2.57}$$

The reference state is vapor filled and therefore remains at an unswollen radius $r_0$. The surface

free energy of the reference state is therefore given simply by

$$F_s^0 = \gamma_{sv} 2\pi r_0 L_t \,. \tag{2.58}$$

The number of ions $N_p$ in a pore is

$$N_p = A_c S_p = 2\pi r_0 L S_p \tag{2.59}$$

and the number of water molecules in the pore is

$$N_l = \frac{\rho_w}{M_w} V_l = \frac{\rho_w}{M_w} \left(\pi r^2 L + 2\pi r^3 b_\theta\right) \,. \tag{2.60}$$

The mole ratio of liquid water is then

$$X_l = \frac{r^2 L + 2r^3 b_\theta}{2\beta r_0 L + r^2 L + 2r^3 b_\theta} \tag{2.61}$$

where $\beta = S_p M_w / \rho_w$ .

For the swelling of a cylindrical pore we constrain $L_t$ such that $\alpha_1 = 1$. The stretching of the length of the perimeter of the cylinder $\alpha_2 = r/r_0$. Because we assume $V_m = V_m^0$, then $\alpha_1 \alpha_2 \alpha_3 = 1$ therefore $\alpha_3 = 1/\alpha_2$. Equation (2.45) becomes

$$\Delta F_{el} = \frac{kT\pi r_0^2 L_t A_v}{2\phi \bar{V}_m^T} \left[ \left(\frac{r}{r_0}\right)^2 + \left(\frac{r_0}{r}\right)^2 - 2 \right] \tag{2.62}$$

Now $m_p$, $V_l$, $F_s$, $F_s^0$, $X_l$ and $\Delta F_{el}$ are substituted into (2.43) which yields,

$$\begin{aligned}\mathcal{G}-\mathcal{G}^0 = &\left[(p-p_{sat})+\frac{R_wT}{v_l}\ln\left(\frac{r^2L+2r^3b_\theta}{p_r\left[2\beta r_0L+r^2L+2r^3b_\theta\right]}\right)\right]\left(\pi r^2L+\frac{2\pi r^3}{3}b_\theta\right)\\ &+R_uT\left[\ln\left(1-\frac{r^2L+2r^3b_\theta}{2\beta r_0L+r^2L+2r^3b_\theta}\right)+\frac{r^2L+2r^3b_\theta}{2\beta r_0L+r^2L+2r^3b_\theta}\chi_{pl}\right]2\pi r_0LS_p\\ &+\frac{kT\pi r_0^2L_tA_v}{2\phi\bar{V}_m^T}\left[\left(\frac{r}{r_0}\right)^2+\left(\frac{r_0}{r}\right)^2-2\right]+\gamma_{sv}2\pi(r-r_0)L_t-2\pi rL\gamma_{lv}\cos\theta+2\gamma_{lv}\pi r^2a_\theta\,. \quad (2.63)\end{aligned}$$

Equation (2.63) is the governing equation for the cylindrical system. It is entirely defined by the geometric parameters $L$ and $r$ and the state variables $p$ and $T$ which are imposed on the system.

### 2.3.1 Capillary Pressure

We briefly consider the surface pressure in a cylindrical pore. Substituting our definition of $F_s$ (2.57) into (2.30) yields

$$p_s=\frac{\partial F_s}{\partial V_l}=\frac{\partial}{\partial V_l}\left[\gamma_{sv}2\pi rL_t-2\pi rL\gamma_{lv}\cos\theta+2\gamma_{lv}\pi r^2a_\theta\right]\,. \quad (2.64)$$

If $r$ is constrained to $r_0$, and the liquid volume $V_l$ can grow in $L$ as the column of water extends down the pore, then

$$p_s=\frac{\partial F_s}{\partial V_l}=\frac{\partial F_s}{\partial L}\frac{\partial L}{\partial V_l}=-\frac{2\gamma_{lv}\cos\theta}{r_0}\,, \quad (2.65)$$

which is the classical Laplace equation for capillary pressure.

## 2.4 Spherical System

In a similar manner we impose the spherical geometry onto the equilibrium conditions. The mass of the protons in the mixture is given by the area of the liquid agglomeration in contact

with the backbone and the density of the sulfonate sites on that surface,

$$m_p = M_p S_p n 4\pi r_0^2. \tag{2.66}$$

The spherical agglomeration of liquid water has partial contact with the Nafion backbone such that the area of the solid-liquid interface is $nA_l$ and the area of the liquid-vapor interface is then $(1-n)\,A_l$. The surface energy from (2.50) can be written as

$$F_s = \gamma_{sl} n 4\pi r^2 + \gamma_{lv}\,(1-n)\,4\pi r^2 + \gamma_{sv} A^c \tag{2.67}$$

where $A^c$ represents the constant area of the backbone that contacts only vapor.

The free energy of the vapor filled reference state is given by

$$F_s^0 = \gamma_{sv} n 4\pi r_0^2 + \gamma_{sv} A^c. \tag{2.68}$$

The number of ions $N_p$ in the sphere is

$$N_p = n 4\pi r_0^2 S_p\,, \tag{2.69}$$

and the number of water molecules in the sphere is

$$N_l = \frac{\rho_w}{M_w} V_l = \frac{\rho_w}{M_w}\frac{4}{3}\pi r^3\,. \tag{2.70}$$

The mole ratio of liquid water is then

$$X_l = \frac{r^3}{r^3 + 3\beta n r_0^2} \tag{2.71}$$

where $\beta = S_p M_w/\rho_w$ as before.

As in the cylindrical geometry, we assume that the term $g_p(p) - g_p^0(p)$ term is negligible, and we assume that when the membrane swells, the volume of the membrane backbone itself remains constant, $V_m = V_m^0$. For the change in free energy we use Flory's elastic term (2.45). For the swelling of a spherical pore $\alpha_1 = r/r_0$, $\alpha_2 = r/r_0$ and with $V_m = V_m^0$, then $\alpha_1\alpha_2\alpha_3 = 1$ therefore $\alpha_3 = (r_0/r)^2$. With (2.48), the elastic free energy (2.45) then becomes

$$\Delta F_{el} = \frac{2kT\pi r_0^3 L_t A_v}{3\phi \bar{V}_m^T}\left[2\left(\frac{r}{r_0}\right)^2 + \left(\frac{r_0}{r}\right)^4 - 3\right], \tag{2.72}$$

for a spherical pore.

We substitute $m_p$, $V_l$, $F_s$, $F_s^0$, $X_l$ and $\Delta F_{el}$ into (2.43) which yields,

$$\begin{aligned}\mathcal{G} - \mathcal{G}^0 = &\left[(p - p_{sat}) + \frac{R_w T}{v_l}\ln\left(\frac{r^3}{p_r\left[r^3 + 3\beta n r_0^2\right]}\right)\right]\frac{4}{3}\pi r^3 \\ &+ R_u T \ln\left(1 - \frac{r^3}{r^3 + 3\beta n r_0^2}\right) S_p n 4\pi r_0^2 + \frac{2kT\pi r_0^3 L_t A_v}{3\phi \bar{V}_m^T}\left[2\left(\frac{r}{r_0}\right)^2 + \left(\frac{r_0}{r}\right)^4 - 3\right] \\ &+ \gamma_{sv} n 4\pi(r^2 - r_0^2) + \gamma_{lv}(1 - n - n\cos\theta)4\pi r^2 . \end{aligned} \tag{2.73}$$

Equation (2.73) is our governing equation for the spherical pore.

# Chapter 3

# Finding Minima

In the previous section we determined governing equations for the total free energy of both a cylindrical pore (2.63), and a spherical pore (2.73). In this section we constrain the radius of the pore to determine whether liquid or vapor is favourable. Since in our formulation we subtract the constant free energy of a vapor filled pore $\mathcal{G}^0$, we know that if $\mathcal{G} - \mathcal{G}^0$ is negative then liquid is favorable, if not then the free energy of vapor is lower and thus vapor is favorable. After determining conditions for liquid sorption we define a channel such that sorption occurs to determine the level in which the pore swells.

To compute the surface density of protons we assume $S_p = C\left(\bar{V}_m^T \cdot S\right)^{-1}$, where $\bar{V}_m^T$ is the specific molar volume of the membrane, $S$ is the specific pore surface area, and $C$ is a constant we use to vary the value. We take the values, $\bar{V}_m^T = 537\, cm^3/mol$ and $S = 210\, m^2/cm^3$ for Nafion 117 from [38], and [34], respectively; with $C = 1$, $S_p = 8.87 \times 10^{-6}\, mol/m^2$. To compute $\mathcal{G} - \mathcal{G}^0$ we use a value of $\theta = 98°$ taken from Zawodzinski et al. [52], which was measured at $p_r = 1$. As mentioned earlier Zawodzinkski et al. finds that $\theta$ varies with water content; however, we are primarily concerned with hydration near saturation therefore we hold $\theta$ constant. The measurement of varying contact angle perhaps couples the attraction of the protons with the repulsion of the backbone and should be investigated.

## 3.1 Fluid Phase Stability Criteria

### 3.1.1 Unswollen Cylindrical Pores

In the following we consider unswollen pores to determine which regions of the membrane would contain liquid water in equilibrium, at a given pressure and temperature. When the pore is not swollen $r = r_0$ and the total free energy of the cylindrical pore, (2.63) becomes

$$\mathcal{G} - \mathcal{G}^0 = 2\pi r_0 L \left\{ \frac{r_0}{2} \left[ (p - p_{sat}) + \frac{R_w T}{v_l} \ln\left(\frac{X_l}{p_r}\right) \right] + R_u T \ln\left(1 - X_l\right) S_p - \gamma_{lv} \cos\theta \right\} + f_{end} \,. \tag{3.1}$$

The last term is an abbreviation for

$$f_{end} = \left[ (p - p_{sat}) + \frac{R_w T}{v_l} \ln\left(\frac{X_l}{p_r}\right) \right] \frac{2\pi r_0^3}{3} b_\theta + 2\gamma_{lv} \pi r_0^2 a_\theta \,; \tag{3.2}$$

it represents the end effects, which is the energy of the lentil that is present when $L = 0$.

Figure 3.1 shows $\mathcal{G} - \mathcal{G}^0$ against $L$ for various pore radii in saturated conditions ($p_r = 1$). We see in the figure that the free energy is essentially independent of $L$ at a certain critical pore radius which we compute to be $r_c = 0.492\,\mathring{A}$. For all pores wider than this, growth of a liquid agglomeration reduces the free energy of the system. However, $L$ must be larger than a certain critical value $L_{crit}\,(r)$ for liquid stability: indeed, stability for liquid occurs when $\mathcal{G} - \mathcal{G}^0$ is negative, so that the free energy of liquid is lower than that of vapor. Therefore, the critical length $L_{crit}\,(r)$ is obtained as the solution of $\mathcal{G} - \mathcal{G}^0 = 0$. In Figure 3.2 we plot $L_{crit}\,(r)$ vs $r$ with $p_r = 1$. Pores must be longer than the critical length for a certain pore width, $L_t > L_{crit}\,(r)$, in order to fill with liquid. If so, they will fill completely since then the minimum of $\mathcal{G} - \mathcal{G}^0$ is obtained for $L$ as large as possible, as can be seen in Figure 3.1. If the pore fills completely, it will stretch radially until balanced by the elastic energy. For very narrow channels, with radii smaller than $r_0 = 0.1\,nm$, liquid stability is unlikely, since the critical length required for a pore

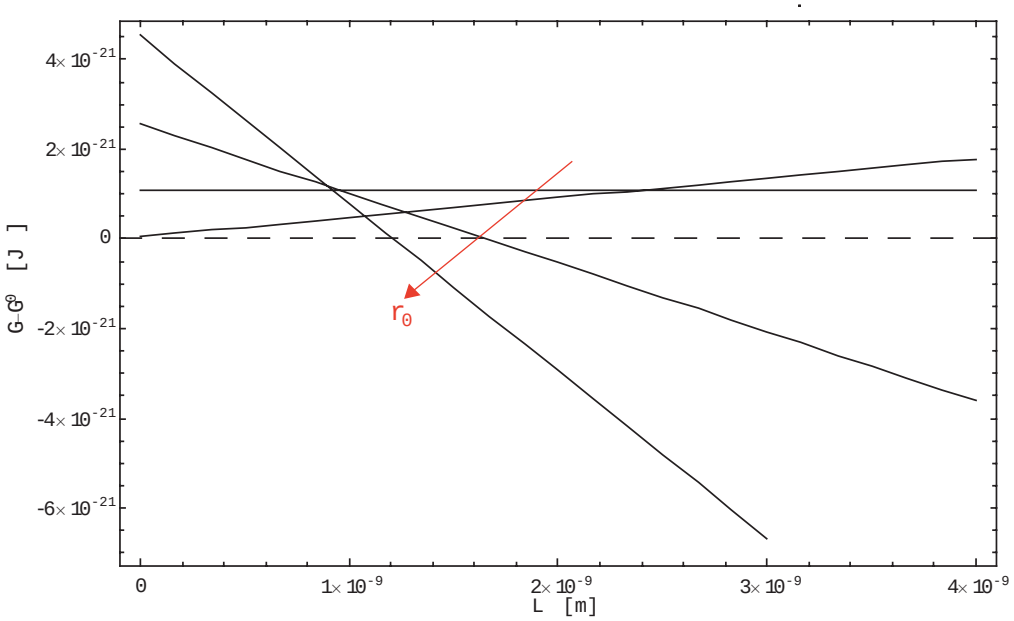


Figure 3.1: Total Free Energy vs $L$ $\left(r_0 = 0.1\,\mathring{A}\text{: }1\,\mathring{A}\right)$ - Cylindrical Pore.

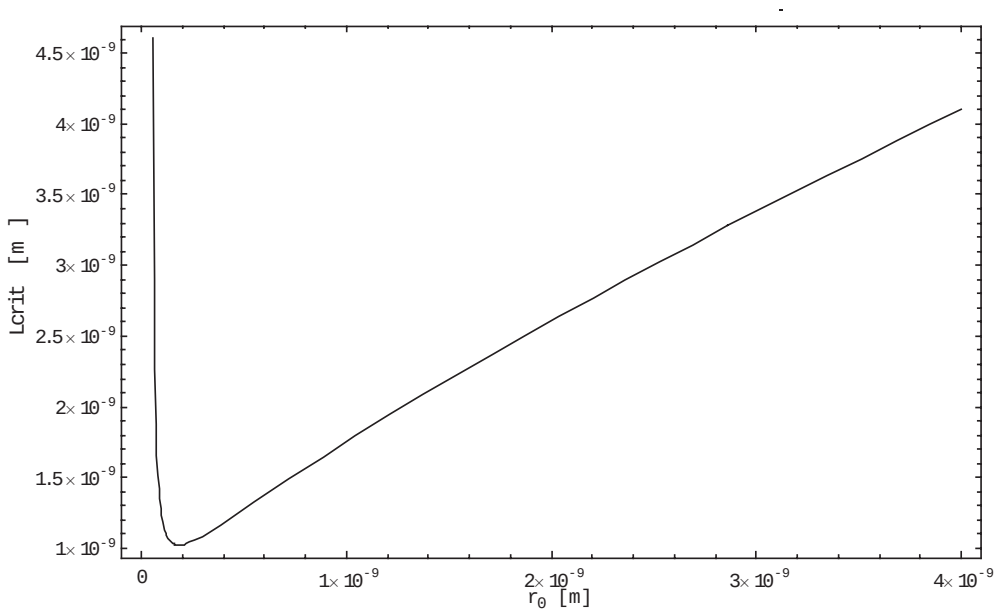


Figure 3.2: Critical Length vs $r_0$ - Cylindrical Pore.

becomes very large (Figure 3.2). This is because entropic effects, which favor liquid, scale with volume, while the surface forces, which favor vapor, scale with surface area. In pores with very small radii, the surface forces dominate. Experimentally measured 'clusters' of radii $5 - 25\,\mathring{A}$, observed in various diffraction and microscopic studies [19], are certainly within the calculated range of stability.

It is important to focus mainly on the trends in the plots as the values are sensitive to the parameters chosen, such as surface density of sulfonate sites and contact angle of the backbone. The surface density of sulfonate sites was computed using the pore-specific surface value proposed by Divisek et al. using SPM methods [34]. In their calculation Divisek et al. assume the entire volume of micropores to be composed of pores with a radius of 1nm. Although differential curves of pore surface area seem to imply a sharp peak in the contributions to surface area centered around pores of radii of 1.5 nm, the value used for $S_p$ can only be taken as an approximation if indeed the SPM method produces accurate results. Also it is generally thought that there is not a uniform distribution of sulfonate sites in the membrane when considering the micro/nano scale [6]. In light of these assertions we plot the critical liquid length versus radius while varying the sulfonate site density in Figure 3.3. We find the expected result, that when the density of sulfonate sites is decreased, there is a corresponding increase in the critical radius for sorption and also an increase in the critical length for a given $r_0 > r_c$.

The value of the contact angle of the pore 'surface' can also only be considered an approximation. In the oft cited work by Zawodzinski et al., the contact angle of liquid water and Nafion was measured at the surface of the membrane where the properties may be dissimilar to those within the membrane. It has been proposed that the membrane may be covered with a nanoscopic hydrophobic 'skin' [52][36]. Certainly the results reported by Zawodzinski et al. carry some question marks with them. The fact that the receding angle measured was often negligible and that the contact angle was found to vary dramatically with $p_r$ seems to indicate that the

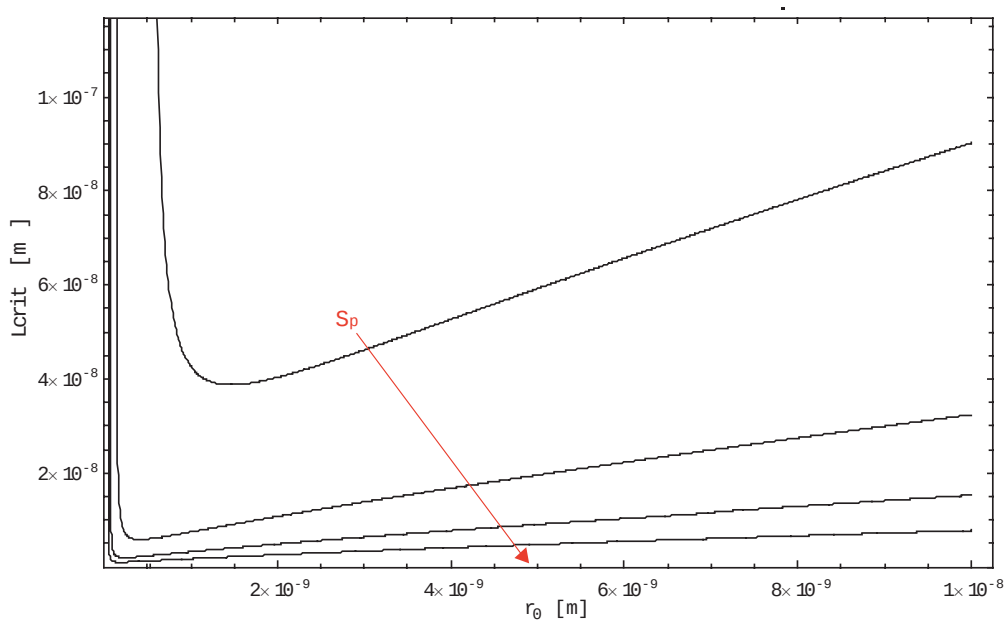


Figure 3.3: Critical Length vs $r_0$ (varying $S_p$ with $C = 1, 1/2, 1/4, 1/8$) - Cylindrical Pore.

measurement of the surfaces forces present can not be extricated from the influence of the other thermodynamic forces present (using the contact angle of Teflon might be more appropriate). In Figure 3.4 we show the critical length versus radius for contact angles of $\theta = 98°, 107°, 116°$ as measured by Zawodzinski[1]. We see that when the contact angle is increased there is a corresponding increase in the critical radius for sorption and also and increase in the critical length for a given $r_0 > r_c$. A larger contact angle indicates a greater degree of hydrophobicity and we see consequently, a stronger desire for the surface to form a solid-vapor interface. To compensate entropic forces must be higher for liquid to remain stable and since the entropic forces scale with volume thus we see an increase in the critical length and critical radius as a result.

Figure 3.5 shows $L_{crit}\,(r)$ for various pressure ratios $p_r$. The curves indicate that the stability of

[1] The values of $\theta = 98°, 107°, 116°$ were measured at $p_r = 1, 0.82, 0$ respectively; however, we vary only $\theta$ but not $p_r$ here.

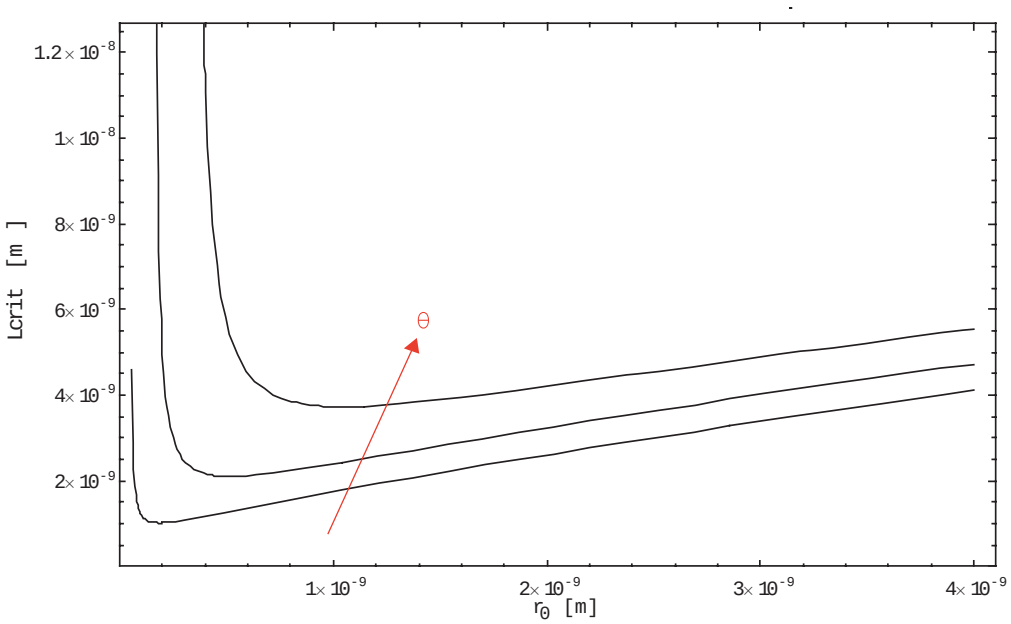


Figure 3.4: Critical Length vs $r_0$ ($\theta = 98°, 107°, 116°$) - Cylindrical Pore.

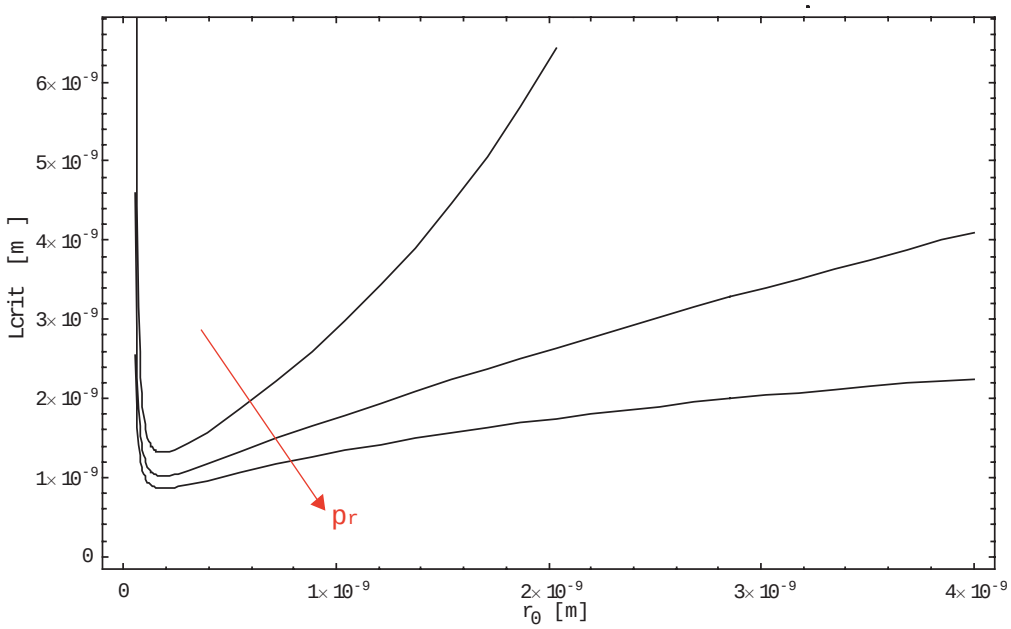


Figure 3.5: Critical Length vs $r_0$ ($p_r = 0.8 : 1.2$) - Cylindrical Pore.

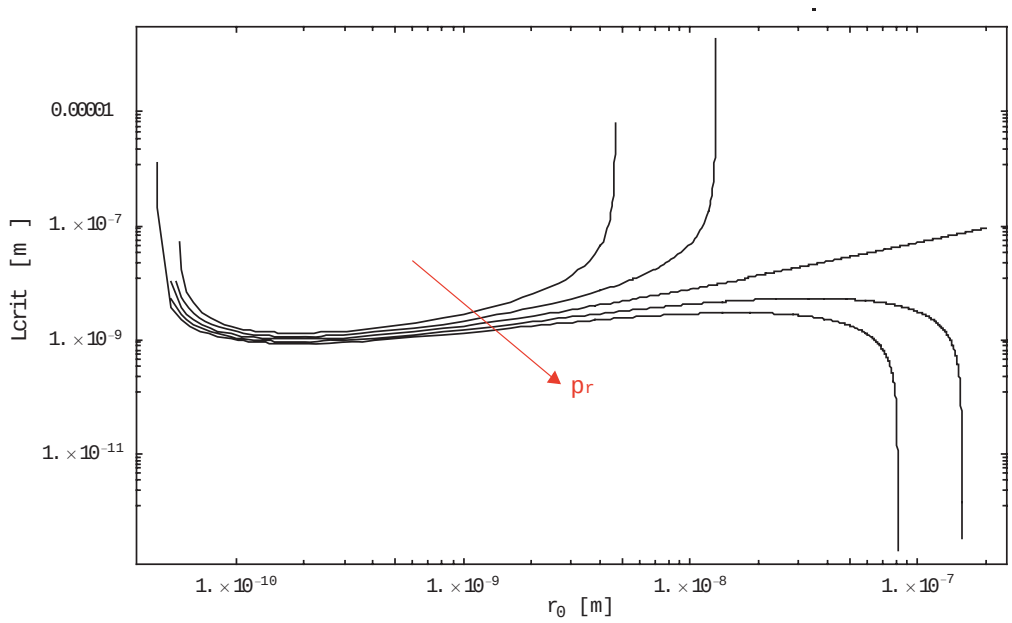


Figure 3.6: Critical Length vs $r_0$ ($p_r = 0.8 : 1.2$) - Cylindrical Pore.

liquid depends on the external pressure. The effects of the pressure ratio $p_r$ are much stronger for wider pores, where the entropic effects begin to dominate. Figure 3.6 presents a log-log plot over a wider range of values that shows this trend to a greater degree. We see that in under-saturated environments very wide pores become totally unstable, regardless of length, while in over-saturated environments, the opposite is true, very wide pores become stable, for any filling length. These plots indicate that the water content in Nafion is drastically reduced in under-saturated environments, as shown in [53]. We propose that the interconnection of liquid pathways would sharply decrease due to under-saturation, which explains the drastic reduction in conductivity of the membrane in under-saturated states [2].

Recall that we only consider pores where liquid fills the whole pore radius, and consider variations in $L$ which would lead to a lower free energy than the vapor filled state. We do not consider liquid agglomeration of radii lower than the unswollen pore diameter, $r < r_0$. These situations are considered unlikely to be stable due to the high interfacial energy between liquid

and vapor.

The above observations concern equilibrium states. Liquid agglomerations would have to transition through unstable configurations when filling a pore to reach a final stable state. In a similar analogy, a droplet of rain in the atmosphere transitions to a critical radius in which growth is favorable, through smaller unstable radii, with the help of a particle of dust [43]. The intermediate non-equilibrium states in the membrane are certainly interesting but are not considered here.

### 3.1.2 Schroeder's Paradox

Here we consider various scenarios in which the end effects are altered. Due to complexity which arises in such cases, we restrict these analyses to comparisons of full, $L = L_t$, or empty cylindrical pores $L = 0$. In these scenarios we use the physical constants specified at the start of the chapter, and consider only saturated conditions ($p_r = 1$).

If a channel were to form a closed loop within the membrane, then the effects of the liquid-vapor interface would be dropped, if we consider only the case when the channel is either full ($L = L_t$). In such a situation $f_{end}$ does not appear in (3.1) and we are left with

$$\mathcal{G} - \mathcal{G}^0 = 2\pi r_0 L_t \left\{ \frac{r_0}{2} \left[ (p - p_{sat}) + \frac{R_w T}{v_l} \ln\left(\frac{X_l}{p_r}\right) \right] + R_u T \ln\left(1 - X_l\right) S_p - \gamma_{lv} \cos\theta \right\} . \quad (3.3)$$

The mole ratio becomes

$$X_l = \frac{r_0 \xi}{2 + r\xi} \quad (3.4)$$

where $\xi = \beta^{-1}$.

We can rearrange the term in the square brackets

$$(p_{sat} - p) + \frac{R_w T}{v_l} \ln\left(\frac{X_l}{p_r}\right) = p_{sat}\left[1 - \frac{p}{p_{sat}} + \frac{R_w T}{p_{sat} v_l} \ln\left(\frac{X_l}{p_r}\right)\right] = p_{sat}\left[1 - p_r + \frac{v_v}{v_l} \ln\left(\frac{X_l}{p_r}\right)\right]. \tag{3.5}$$

We know

$$1 - p_r << \frac{v_v}{v_l} \ln\left(\frac{X_l}{p_r}\right) \tag{3.6}$$

because $v_v/v_l$ is on the order of $10^3$ and therefore the $(p - p_{sat})$ is negligible. We find then, that the solution of

$$\frac{r_0}{2} \frac{R_w T}{v_l} \ln\left(\frac{r_0 \xi}{p_r\left[2 + r_0 \xi\right]}\right) + R_u T \ln\left(1 - \frac{r_0 \xi}{2 + r_0 \xi}\right) S_p - \gamma_{lv} \cos\theta = 0 \tag{3.7}$$

for $r_0$ yields a critical radius for the stability of liquid which is $r_c = 0.049\,\mathring{A}$. If $r_0 < r_c$, (3.3) is minimum with vapor and if $r_0 > r_c$ then liquid at $L = L_t$ is favorable. This critical radius is negligibly small, in a range where the continuum nature of this analysis is no longer valid. We see then that we would expect such a loop to be always stable in equilibrium which indicates that the entropic forces are more influential than the energetic interfacial forces in such a scenario.

We also consider the case where a liquid pore ends in a dead end. In this case, the surface area of one end is considered to have a solid-liquid interface, while the other remains a liquid-vapor interface. Fig. 3.7 shows the difference in stability requirements if one liquid-vapor interface is eliminated. The critical length for this case is considerably smaller than for the case where both ends are in contact with vapor. This shows that a pore with one side fills easier than one which is bounded by liquid-vapor on both ends.

The most important alternate scenario we consider is the case where the membrane is bounded by saturated liquid rather than saturated vapor. In such a case, when the pore is full of liquid,

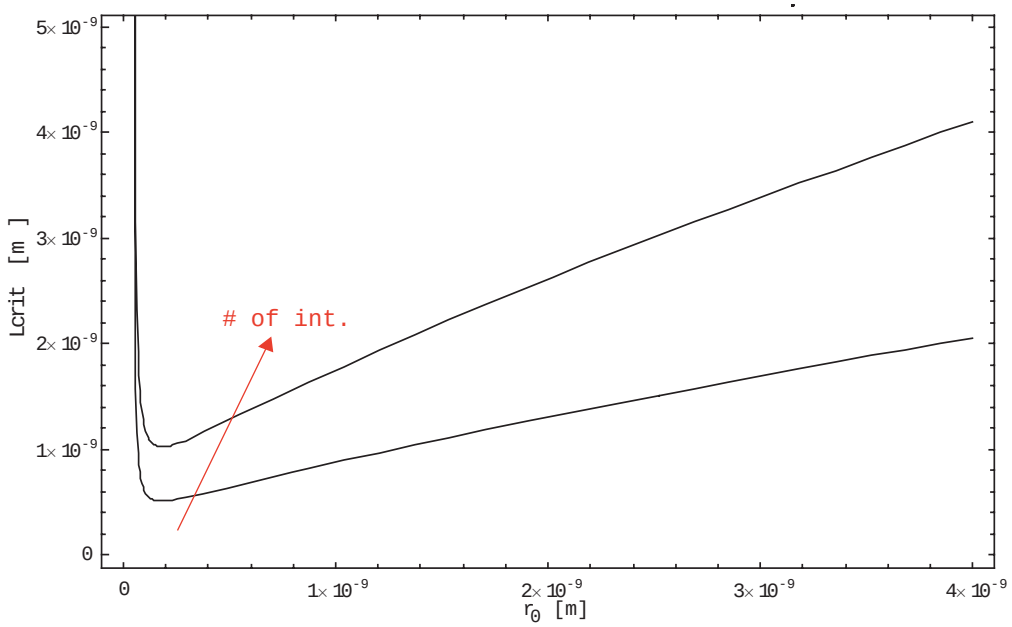


Figure 3.7: Critical Length vs $r_0$ (with 1 and 2 Liquid Vapor Interfaces) - Cylindrical Pore.

there exists no liquid-vapor interface; however, if the pore is empty there exists a liquid-vapor interface identical to that of a liquid filled pore in a saturated vapor environment. In such a case the sign of the free energy of the end effects changes, $f_{end} = -2\gamma_{lv}\pi r_0^2 a_\theta$, and the free energy of the system becomes

$$\mathcal{G} - \mathcal{G}^0 = 2\pi r_0 L_t \left\{ \frac{r_0}{2} \left[ (p - p_{sat}) + \frac{R_w T}{v_l} \ln\left(\frac{X_l}{p_r}\right) \right] + R_u T \ln\left(1 - X_l\right) S_p - \gamma_{lv} \cos\theta - \gamma_{lv} a_\theta \frac{r_0}{L_t} \right\} . \tag{3.8}$$

In this case we find a dependence on the ratio of the pore radius to the pore length as expressed in the final term of (3.8). In the limit of the length of the pore being very large in comparison to the radius, then we get the first scenario discussed, where $f_{end}$ goes to zero. As the ratio becomes significant, it serves to further reduce the critical radius from $r_c = 0.049\,\mathring{A}$, which was already negligibly small. Therefore we find that in saturated liquid, sorption of the liquid water phase is dominant. This serves to explain how Nafion absorbs significantly more water in a saturated liquid environment. It is important to note however that the phenomenon of

Schroeder's paradox is not necessarily coupled with a porous structure, as detailed in [54]. Nevertheless, we see here that given a porous structure we can expect a considerable difference in sorption with a change in the phase at the boundary.

### 3.1.3 Unswollen Spherical Pores

We now consider the case of spherical pores; we again restrict the analysis to rigid pores with $r = r_0$ in the governing equation for the total free energy of a spherical pore system (2.73), which yields

$$\mathcal{G} - \mathcal{G}^0 = \left[(p_{sat} - p) + \frac{R_w T}{v_l} \ln\left(\frac{X_l}{p_r}\right)\right] \frac{4}{3}\pi r_0^3 + R_u T \ln(1 - X_l)\, 4\pi r_0^2 S_p n + [(1 - n) - n\cos\theta]\, \gamma_{lv} 4\pi r_0^2\,, \quad (3.9)$$

with

$$X_l = \frac{r_0}{r_0 + 3\beta n}\,. \quad (3.10)$$

Figure 3.8 shows (3.9) plotted against $r_0$ for values of surface coverage $n = 0.4, 0.5, 0.6$. Recall that the surface coverage represent the ratio of solid-liquid interaction to the total area of the liquid droplet, whereas $1 - n$ represents the ratio of the pore that is open to channels, yielding a liquid-vapor interface for a liquid filled pore. Since $r$ is restricted to $r_0$ this plot represents droplets of various sizes throughout the membrane, not droplet growth. We see in the plot that as the surface coverage increases the critical radius for the stability of liquid decreases. These results may seem counterintuitive at first glance, considering that Nafion is a hydrophobic surface; however, (3.9) stipulates that as we increase surface coverage (i.e. solid-liquid interface) we decrease liquid-vapor interface $(1-n)$ proportionally. The factor $\cos\theta$ therefore means that an increase in the solid-liquid interface will have a lesser effect on the total free energy of the system than the corresponding decrease of the liquid-vapor interface.

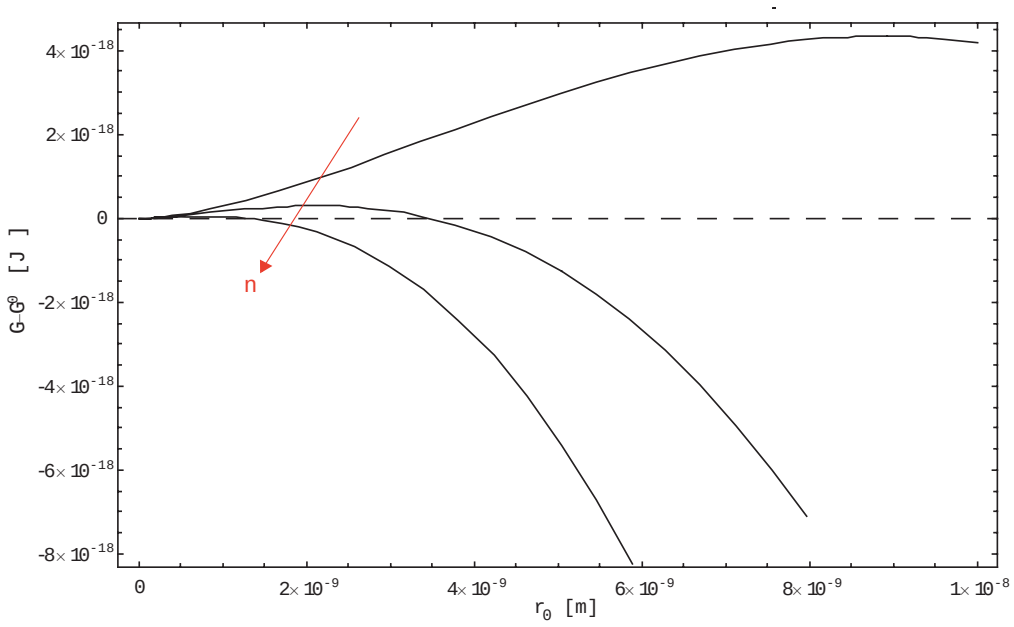


Figure 3.8: Total Free Energy vs $r_0$ ($n = 0.4, 0.5, 0.6$) - Spherical Pore.

Increasing the surface coverage also increases the fraction of protons to water molecules that are in the mixture. In Figure 3.8 we see that for a fractional surface coverage of $n = 0.6$, liquid is stable in regions of radii larger than approximately $1.3\,nm$. If we decrease the surface coverage to $n = 0.5$, the stability criterion for liquid stability shifts to $3.4\,nm$ and even higher values for further decreasing coverage. Conversely, as the surface coverage goes to $n = 1$, i.e., no liquid-vapor interface at all, the critical radius is negligibly small ($0.75\,\mathring{A}$), similar to the case of a cylindrical pore in a closed loop. We see again that at saturation ($p_r = 1$) the entropic desire for liquid dominates the hydrophobic repulsion of backbone surface. The inclusion of a liquid-vapor interface strongly impacts the system and we see that larger agglomerations are required for stability with decreasing surface coverage.

### 3.1.4 Cluster and Channel Configuration

The cluster-channel morphology introduced by Gierke et al. (see Figure 1.6) can be deconstructed into the cylindrical and spherical pores discussed above. For a channel separating two clusters, the energetics of the clusters would be described as above with $n$ equal to the ratio of the area of polymer interface over the total area of the spherical region. From the dimensions shown in Figure 1.6, this would imply $n \approx 0.95$, and therefore liquid would be very favorable in saturated conditions. A channel between two liquid filled clusters is indeed equivalent to a cylindrical pore that is bounded by saturated liquid. From that analysis we know that in saturated conditions a liquid filled channel is energetically very favorable in comparison to vapor filled. It is also interesting to note, that if the clusters were not liquid filled, the channel between the clusters ($L = 1\,nm$ and $r_0 = 0.5\,nm$) would not be filled with liquid as well (see Figure 3.2). What we see then, in general, is that with the geometry described by Gierke et al., shown in Figure 1.6, spherical pores (or clusters) will fill first, and if there is a cylindrical pore (channel) joining two clusters it will then proceed to fill. It is important to stress the effect of the parameters $\theta$, and $S_p$, which we described as approximate. In Figure 3.9 we show the stability criteria can change by plotting the free energy of a spherical pore of $n = 0.95$, with $\theta = 107^\circ$ and $C = 1, 1/2, 1/4$. We see that an increase in contact angle, and a decrease in sulfonate site density, dramatically increases the critical radius for the stability of the liquid phase.

## 3.2 Pore Swelling

In this section we prescribe an initial configuration, for a cylindrical pore and a spherical pore, such that the pore will be filled with liquid, according to the analysis in the previous section. We then allow the pore to swell past the initial radius in order to observe the effects of the deformation of the membrane on the total free energy of the system.

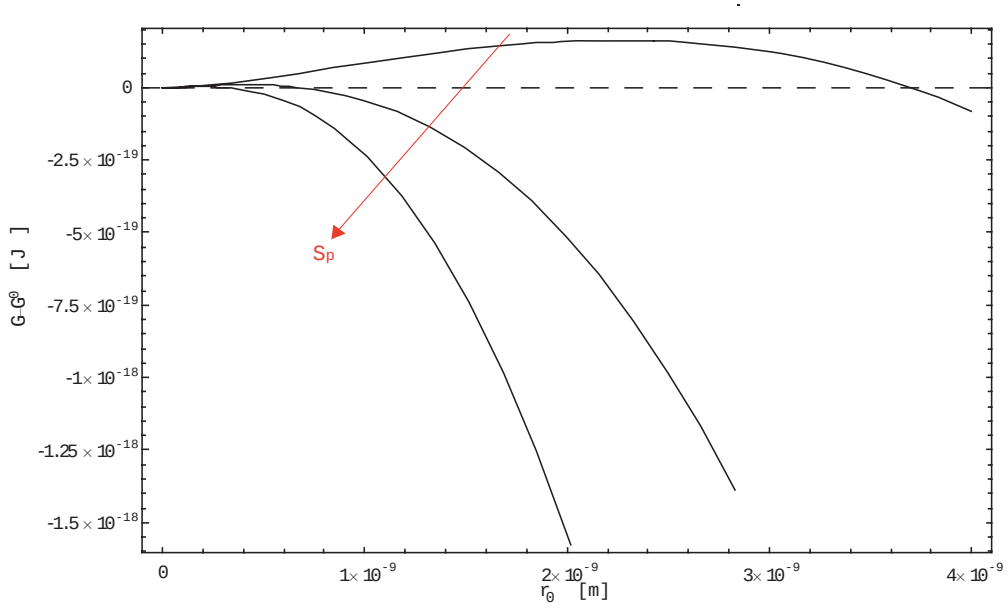


Figure 3.9: Total Free energy vs $r_0$ ($\theta = 107°$ and $C = 1, 1/2, 1/4$) - Spherical Pore.

### 3.2.1 Cylindrical Pore Swelling

Liquid growth in $L$ is constrained to boundary minima, at either $L = L_t$ or $L = 0$ (see Figure 3.1). A full pore will, however, begin to swell, to $r > r_0$, in order to take on more water and thus increase the entropy of mixing, but this also increases the free energy, due to an increase in interfacial surface area, and due to the swelling of the membrane. Nafion is known to swell significantly in the presence of water. The pore comes to an equilibrium point in $r$ when the change in free energy of the membrane due to swelling balances the entropic desire to take on more water.

To compute the amount of swelling for a given pore we use the governing equation for the total free energy of a cylindrical pore system (2.63) with the same values of the constants as before, $\theta = 98°$, $p_r = 1$, $\chi_{pl} = 0$, $\bar{V}_m^T = 537\,cm^3/mol$, $S = 210\,m^2/cm^3$, $T = 300\,K$. Moreover, we assume that the solid-vapor surface tension is negligibly small and accordingly set $\gamma_{sv} = 0$. We specify the geometry of the undeformed pore as $r_0 = 0.5nm$, and $L_t = 2\,nm$. We use Gierke

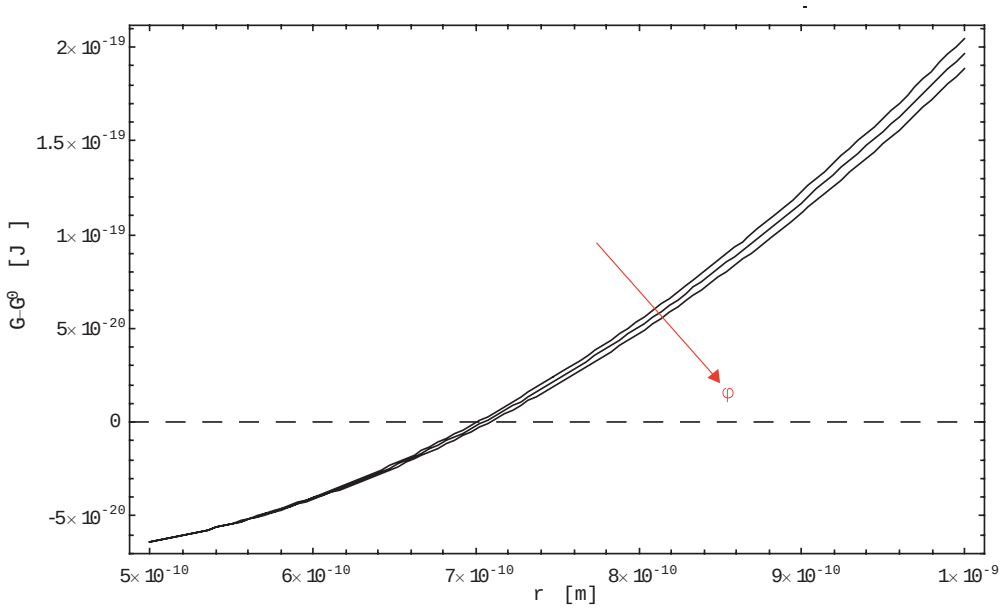


Figure 3.10: Total Free Energy vs $r$ ($\phi = 1/2, 1/3, 1/4$) - Cylindrical Pore ($r_0 = 0.5\,nm$, $L_t = 2\,nm$).

et al.'s radius but double the length of the pore (see Figure 1.6) to ensure the stability of the liquid phase as indicated in Figure 3.2. The porosity of the membrane, $\phi$, specifies the ratio of the undeformed pore size to the amount of membrane that it stretches as given by (2.47).

In Figure 3.10 we plot the $\mathcal{G} - \mathcal{G}^0$ as a function of $r$ for values of $\phi = 1/2, 1/3, 1/4$. We see that despite the liquid filled state being favorable, no swelling would occur, which is contrary to experimental evidence. The problem is that we specify that the channel will swell uniformly, which would cause the liquid-vapor interface to grow along with the channel radius. The liquid-vapor interface is a dominant contribution to the free energy and therefore the total free energy of the system grows when $r$ is increased. In all likelihood, we presume, the channel would rather deform in an irregular fashion, keeping the liquid-vapor interface relatively constant. To approximate such a situation, we restrict the liquid-vapor interface to $r_0$, while allowing the rest of the channel to deform to $r$. Figure 3.11 shows the total free energy of the cylindrical pore system with a constant liquid-vapor interface of radius $r_0$ over $r > r_0$ for values of porosity

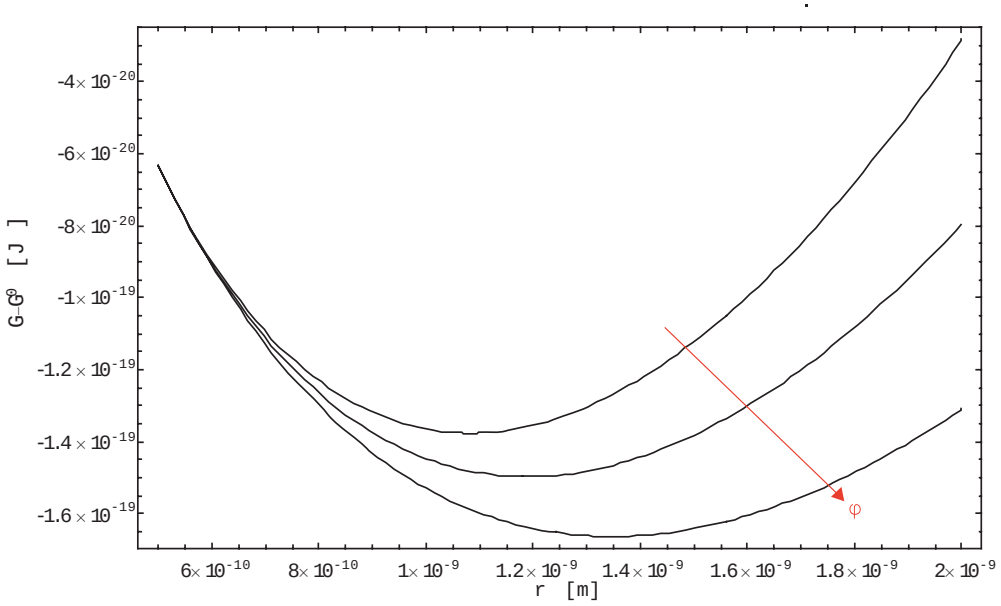


Figure 3.11: Total Free Energy vs $r$ ($\phi = 1/2, 1/3, 1/4$) - Cylindrical Pore ($r_0 = 0.5\,nm$, $L_t = 2\,nm$) with a constant liquid-vapor interface.

$\phi = 1/2, 1/3, 1/4$. The figure shows distinct minima of total free energy at values of $r > r_0$, and increasing with porosity. Increasing porosity implies an decrease in the effective amount of polymer that is deformed, accordingly the equilibrium radius of the swollen pore is increases. At a porosity of 1/2 the pore is deforming to up to three times its radius, which would lead to a two-fold membrane deformation; at a porosity of 1/4 the pore size doubles which would give a 125% growth of the entire membrane[2]. Divisek gives a pore volume to membrane volume ratio of 0.38 for Nafion 117 in a saturated vapor environment, and up to 0.44 for Nafion 112. The value of porosity for Nafion 117 translates to $\lambda = 18.3$ [34], indicating that some of the water is likely surface water; therefore, Nafion 117 is probably in the lower range of porosity values used here.

Keeping the liquid-vapor interface constant is an idealization that is perhaps too great to yield

[2] We relate pore volume to membrane volume using (2.47).

accurate results. Nevertheless, we can see that the contribution of the liquid-vapor interface to total free energy is dominant enough to predict rather non-uniform swelling of a liquid filled cylindrical pore with such an interface. Equation (2.63) shows that the contribution of the liquid-vapor interface, to the total free energy of the system, does not depend on $L_t$ and thus if the length of the liquid in the pore is very large (facilitated by a large $L_t$), compared to the radius of the liquid-vapor interface then the significance of the interface becomes marginal. An example would be if the pore extended from one side of the membrane straight through to the other; then the length of the liquid in the pore would be much greater than the radius ($L_t = 0.1778\,mm$ for Nafion 117), and the swelling would be virtually identical to that shown for a constant liquid-vapor interface.

### 3.2.2 Spherical Pore Swelling

We repeat the analysis for the swelling of a spherical pore. The constants specified above are again used, and the initial radius of the pore is set to $r_0 = 2\,nm$ which is the value set by Gierke and Hsu [21] [3]. In Figure 3.12 we study the swelling of a spherical pore swelling with $\phi = 0.25$ for values of $n = 0.8, 0.95, 1$. We see that no swelling occurs at lower values of the surface coverage parameter $n$, and increases with larger $n$. This, again, shows that the liquid-vapor interface plays a dominant role in swelling behaviour.

For further study, we consider a fixed surface coverage of $n = 0.95$, so that the that the spherical pore has a large solid-liquid interface in comparison to the liquid-vapor interface; this is similar to the Gierke model shown in Figure 1.6. Figure 3.13 shows the total free energy of this pore for varying values of porosity $\phi = 1/2, 1/3, 1/4$. We again see that as the amount of polymer per pore decreases, we see a increase in the final equilibrium radius of the pore, here from $2.35\,nm - 2.6\,nm$, between $\phi = 1/4$ and $1/2$ respectively.

As in the cylindrical case, in an effort to simulate nonuniform swelling, we fix the liquid-vapor

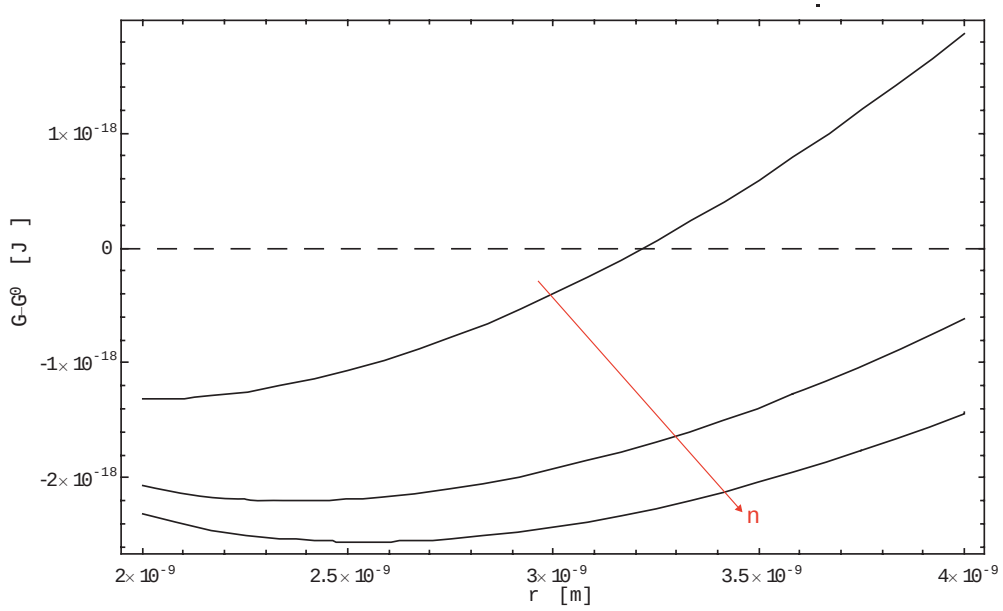


Figure 3.12: Total Free Energy vs $r$ ($n = 0.8, 0.95, 1$) - Spherical Pore ($r_0 = 0.5\,nm$).

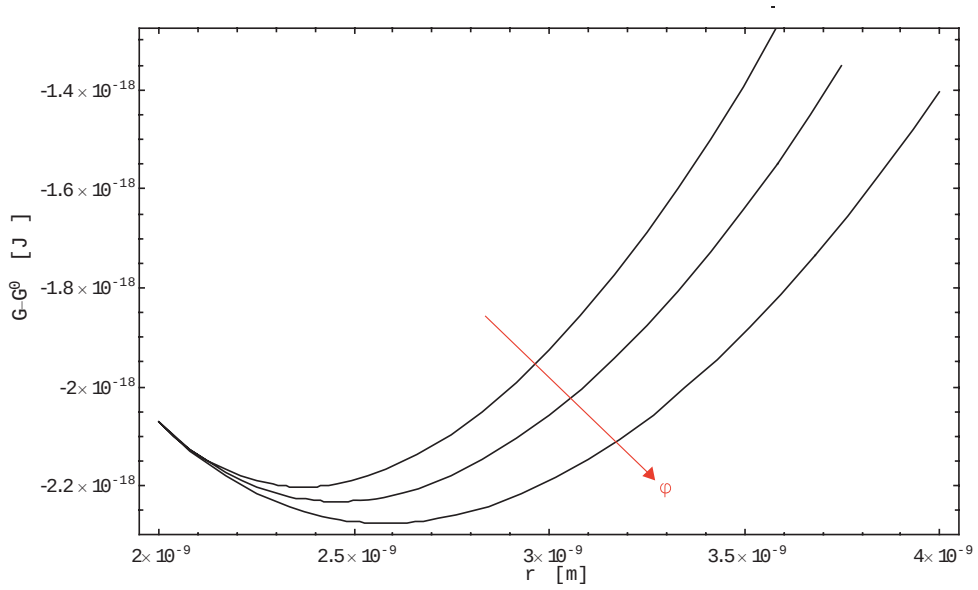


Figure 3.13: Total Free Energy vs $r$ ($\phi = 1/2, 1/3, 1/4$) - Spherical Pore ($r_0 = 0.5\,nm$).

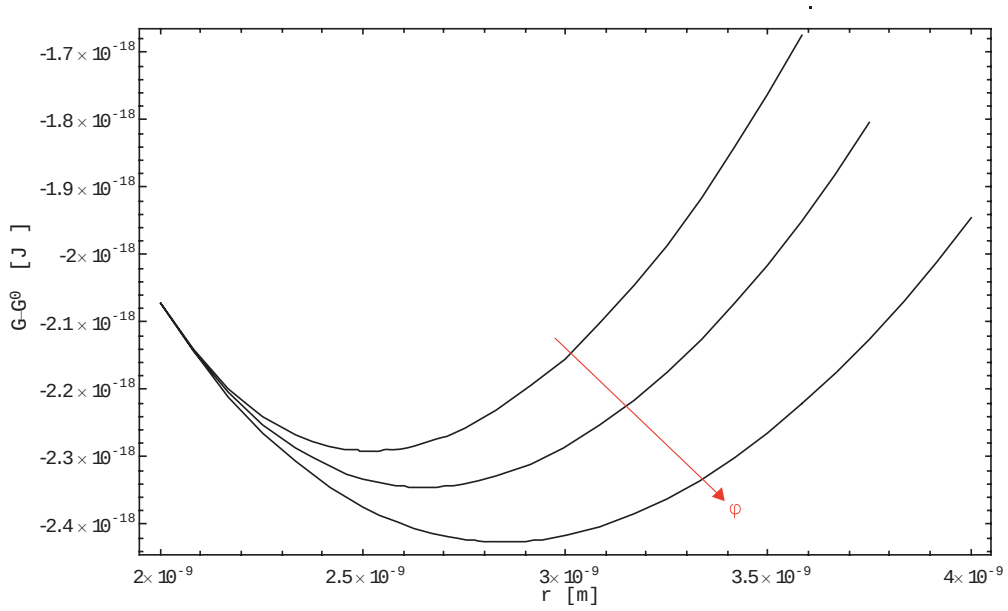


Figure 3.14: Total Free Energy vs $r$ ($\phi = 1/2, 1/3, 1/4$) - Spherical Pore ($r_0 = 0.5\,nm$) with a constant liquid-vapor interface.

interface to be constant. The liquid-vapor interface is held at $(1-n)\,4\pi r_0^2$, while the rest of the pore grows with $r$. Figure 3.14 again shows a spherical pore swelling with $n = 0.95$ for values of $\phi = 1/2, 1/3, 1/4$; however, this time with the liquid-vapor interface constrained. We see somewhat more swelling with this modification, despite the small liquid-vapor interface with $n = 0.95$[3]. We see that the initial radius of $r_0 = 2\,nm$ swells to a radius between $2.5\,nm - 3\,nm$, depending on porosity.

In a similar analysis on the equilibrium size of spherical clusters of water in Nafion [21] [3], Hsu and Gierke find that for Nafion 117, clusters of diameter $3.99\,nm$ should be observed in a saturated environment. Hsu and Gierke do not focus on regions which may support liquid wetting, instead their analysis presupposed uniform dry cluster sizes of $2\,nm$ throughout the membrane, which swell to $4\,nm$ in equilibrium with a saturated vapor. We find somewhat

[3] $n$ is defined at $r_0$, since we are holding the liquid-vapor interface constant and allowing the pore to grow in $r$, $n$ is effectively increasing as well.

less swelling here with an equilibrium radius of $3\,nm$ or under resulting from our analysis. Hsu and Gierke make the assumption that each cluster stretches an infinite and continuous elastic medium, which is defined by an empirical tensile modulus $G(c)$. Freger points out that approximating the polymer as a Hookean medium to yield an elastic energy for polymer is imprecise [8], we here used a change in free energy derived from the change in entropy of polymer chains as they are stretched [46]; this could explain some of the difference in the results[4].

[4] Hsu and Gierke [3], do not use interfacial tension, define the contact angle or include the entropy of mixing. They instead rely on interaction parameters fitted to experimental data; therefore, it is difficult to decipher where other fundamental differences may lie.

# Chapter 4

# Future Work

In this section we hint at possible future work that could result as a consequence of the theory presented. In the previous section we have shown thermodynamic criteria necessary for the wettability of pore within a Nafion membrane. We presented arguments indicating a critical radius and critical length of a pore. In order for such insight to bear fruit, it is necessary to develop a sufficiently flexible pore size distribution model. The analysis presented here can be coupled with such a model in the development of theory to determine the connectivity of the liquid phase throughout the membrane.

We can think of a pathway for proton transport through the membrane to consist of a series of pores connected in a random manner. The size of the pore determines the bulk-like water content, then the level of resistivity and other transport properties such as electroosmotic flow.

Many transport models are based on a porous assumption, but, due to limited knowledge of details on the morphology of Nafion, a simplified structure is often used such as the parallel pore idealization of Choi and Datta [37]. Eikerling et al. present a transport model based on the cluster-network structure of pores [5]; they rightly predict that some pores will be filled with bulk-like water while others will contain only surface water which hydrates the sulfonate group. They propose a random distribution of these pores but are forced to fit their model using conductivity data for lack of sufficient morphological insight. With the theory presented here the goal is to be able to predict the formation of these pore networks.

A simple analogy of the problem would be to consider a box of randomly sized balls which conduct protons. The critical radius determines if a ball is a good conductor or a poor one; however, the critical radius is a function not only of variables imposed by the environment but also is a function of the state of the surrounding balls and dependant on the ball-size distribution. The complexity of this simple analogy illustrates the difficulty in extending the concept to the microstructure of Nafion.

# Chapter 5

# Conclusions

The conductivity of a Nafion membrane has been shown to depend strongly on the amount of water sorbed. Experimental analysis of membranes has lacked sufficient detail to determine a conclusive morphological model of a Nafion membrane upon sorption. Bulk water can be seen as the upper limit of protonic conductivity, therefore it is important to determine the permeation of bulk-like water throughout the membrane in order to establish rigorous transport models.

In this work we proposed a thermodynamic model for the wetting of idealized membrane pores to gain an understanding of the nature of the liquid phase within a Nafion membrane.

We showed how the wetting of pores in a Nafion membrane is dictated by a competition of energetic and entropic forces. The energetic forces are due to the interfaces present, and accordingly scale with interfacial surface area. The entropic forces arise from mixing and the level of saturation; these forces scale with volume.

It was shown that there exists a critical pore radius below which liquid water is unstable. For a cylindrical pore we found a critical length for any pore size greater than the critical radius; below the critical length, a pore cannot be filled. For a spherical pore we show that the stability of the liquid phase depends strongly on the cross sectional area of channels which are adjacent. This model was also used to show how pressure, relative to saturation, affects liquid agglomeration. We found that for a cylindrical pore in an oversaturated environment the critical length can go to zero, and conversely, in an under-saturated state the critical length can become infinite.

We show how decreasing the surface density of sulfonate sites decreases the entropic desire for liquid water and also how increasing the hydrophobicity of the surface increases the energetic desire for vapor, both leading to an increase of the critical radius and critical length for the stability of liquid.

Our model was used to study how thermodynamic forces change depending on the phase at the pore bounds. The results show that pores bounded by saturated liquid have a much smaller critical radius. This indicates how Nafion sorbs so much more water when in saturated liquid as opposed to saturated vapor (Schroeder's paradox). Similarly, the model shows that a cylindrical channel bounded by two water filled pores is very likely to sorb liquid water as this removes the liquid-vapor interfaces.

Nafion is known to swell as it takes on water. To gain insight into this phenomenon we modeled the swelling of pores on the microscopic level. We showed how, if present, a liquid-vapor interface is a dominant contribution to the total free energy of the system, in particular for short pores. This leads to the assumption that swelling at a pore size level would be non-uniform.

This work, therefore documents the criteria necessary for the permeation of the liquid phase within a Nafion membrane. The results presented should be coupled with a probabilistic pore size distribution model in order to determine the connectivity of the liquid phase throughout the membrane as a function of state variables imposed by the system. In our view this would be a large step towards developing a more rigorous model of proton transport through the membrane.

# References

[1] J. Larminie, A. Dicks, Fuel Cell Systems Explained, John Wiley and Sons, Chichester, West Sussex 2000

[2] J. Fimrite, H. Struchtrup, N. Djilali, Transport Phenomena in Polymer Electrolyte Membranes - I. Modeling Framework, J. Electroch. Soc. 152 (2005) A1804-A1814.

[3] T.D. Gierke, W.Y. Hsu, Ion-Transport and Clustering in Nafion Perfluorinated Membranes, J. Membr. Sci. 13 (1983) 307-326.

[4] G. Gebel, Structural evolution of water swollen perfluorosulfonated ionomers from dry membrane to swollen, Polymer 41 (2000) 5829-5838.

[5] M. Eikerling, A.A. Kornyshev, U. Stimming, Electrophysical Properties of Polymer Electrolyte Membranes: A Random Network Model, J. Phys. Chem. B 101 (1997) 10807-10820.

[6] K.A. Mauritz, R.B. Moore, State of Understanding of Nafion, Chem. Rev. 104 (2004) 4535-4585.

[7] A. Zecchina, F. Geobadlo, G. Spoto, S. Bordiga, G. Ricchiardi, R. Buzzoni, G. Petrini, Interaction of $H_2O$, $CH_3OH$, $(CH_3)(2)O$, $CH_3CN$, and Pyridine with the superacid perfluorosulfonic membrane Nafion - an IR and Raman study, J. Phys. Chem 99 (1995) 11937.

[8] V. Freger, Elastic energy in microscoically phase-separated swollen polymer networks, Polymer 43 (2002) 71-76.

[9] P. Schroeder, Uber Erstarrungs–und Quellungserscheinungen von Gelatine, Z. Phys. Chem. 45 (1903) 57.

[10] K. Lum, D. Chandler, Phase Diagram and Free Energies of Vapor Films and Tubes for a Confined Fluid, International Journal of Thermophysics 19 (1998) 3

[11] H.K. Christenson, P.M. Claesson, Cavitation and the Interaction between Macroscopic Hydrophobic Surfaces, Science 239 (1988) 390-392.

[12] O. Beckstein, M.S.P. Sansom, Liquid-vapor oscillations of water in hydrophobic nanopores, PNAS, 100 (2003) 7063-7068.

[13] S. Granick, X. Zhang, Y. Zhu, Hydrophobicity at a Janus Interface, Science 295 (2002) 663-666.

[14] K.D. Kreuer, On the complexity of proton conduction phenomena, Solid State Ionics, 136 (2000) 149-160.

[15] P. Choi, N.H. Jalani, R. Datta, Thermodynamics and proton transport in Nafion - II. Proton Diffusion Mechanisms and Conductivity, J. Electrochem. Soc. 152 (2005) E123-E130.

[16] M. Eikerling, A.A. Kornysheve, A.M. Kuznetsov, J. Ultsrup, S. Walbran, Mechanisms of Proton Conductance in Polymer Electrolyte Membranes, J. Phys. Chem. B. 105 (2001) 3646-3662.

[17] J. Fimrite, Transport Phenomena in Polymer Electrolyte Fuel Cells, M.A.Sc Thesis, University of Victoria 2004.

[18] K.D. Kreuer, On the Development of Proton Conducting Materials for Technological Applications, Solid State Ionics 97 (1997) 1-15.

[19] C. Heitner-Wirguin, Recent advances in perfluorinated ionomer membranes: structure, properties and applications, J. Membr. Sci. 120 (1996) 1-33.

[20] T.D. Gierke, G.E. Munn, F.C. Wilson, The morphology in Nafion Perfluorinated Membrane Products, as Determined by Wide-Angle and Small-Angle X-ray Studies, J. Polym. Sci., Polym. Phys. Ed. 19 (1981) 1687-1704.

[21] W.Y. Hsu, T.D. Gierke, Elastic Theory for Ionic Clustering in Perfluorinated Ionomers, 15 Macromolecules (1982) 101-105.

[22] A.Z. Weber, J. Newman, Transport in Polymer-Electrolyte Membranes I. Physical Model, J.Electrochem. Soc. 150 (2003) A1008-A1015.

[23] A.S. Ioselevich, A.A. Kornyshev, J.H.G. Steinke, Fine Morphology of Proton-Conducting Ionomers, J. Phys. Chem B 108 (2004) 11953-11963.

[24] M. Fujimura, T. Hashimoto, H. Kawai, Small-Angle X-Ray Scattering Study of Perfluorinated Ionomer Membranes 2. Origin of Scattering Maximum, Macromolecules 14 (1982) 1309-1315.

[25] M. Fujimura, T. Hashimoto, H. Kawai, Small-Angle X-Ray Scattering Study of Perfluorinated Ionomer Membranes 2. Models for Ionic Scattering Maximum, Macromolecules 15 (1982) 136-144.

[26] H.L. Yeager, A. Steck, Cation and Water Diffusion in Nafion Ion Exchange Membranes: Influence of Polymer Structure, J. Electroch. Soc. 128 (1981) 1880-1884.

[27] M.H. Litt, A reevaluation of Nafion Morphology, Polym. Prepr. 38 (1997) 80.

[28] H.G. Haubold, T. Vad, H. Jungbluth, P. Hiller, Nano structure of Nafion: a SAXS study, Electrochim. Acta 46 (2001) 1559-1563.

[29] B. Dreyfus, G. Gebel, P. Aldebert, M. Pineri, M. Escoubes, M. Thomas, Distribution of the micelles in hydrated perfluorinated ionomer membranes from SANS experiments, J. Phys. (France) 51 (1990) 1341.

[30] G. Gebel, J. Lambard, Small-Angle Scattering Study of Water-Swollen Perfluorinated Ionomer Membranes, Macromolecules 30 (1997) 7914-7920.

[31] K.D. Kreuer, On the development of proton conducting polymer membranes for hydrogen and methanol fuels, J. Membr. Sci. 185 (2001) 29-39.

[32] K.D. Kreuer, S.J. Paddison, E. Spohr, M. Schuster, Transport in Proton Conductors for Fuel-Cell Applications: Simulations, Elementary Reactions, and Phenomenology, Chem. Rev. 104 (2004) 4637-4678.

[33] G. Karimi, X. Li, Electroosmotic flow through polymer electrolyte membranes in PEM fuel cells, J. Power Sources 140 (2005) 1-11.

[34] J. Divisek, M. Eikerling, V. Mazin, H. Schmitz, U. Stimming, Yu. M. Volfkovich, A Study of Capillary Porous Structure and Sorption Properites of Nafion Proton-Exchange Membranes Swollen in Water, J. Electrochem. Soc. 145 (1998) 2677-2683.

[35] N.P. Blake, M.K. Petersen, G.A. Voth, H. Metiu, Structure of Hydrated Na-Nafion Polymer Membranes, J. Phys. Chem B 109 (2005) 24244-242533.

[36] R.S. Mclean, M. Doyle, B.B. Sauer, High-Resolution Imaging of Ionic Domains and Crystal Morphology in Ionomers using AFM Techniques, Macromolecules 33 (2000) 6541-6550.

[37] P. Choi, R. Datta, Sorption in Proton-Exchange Membranes: An Explanation of Schroeder's Paradox. J. Electrochem. Soc. 150 (2003) E601.

[38] P. Choi, N.H. Jalani, R. Datta, Thermodynamics and proton transport in Nafion - I. Membrane swelling, sorption, and ion-exchange equilibrium, J. Electrochem. Soc. 152 (2005) E84-E89.

[39] P. Futerko, I-Ming Hsing, Thermodynamics of Water Vapor Uptake in Perfluorosulfonic Acid Membranes, J. Electrochem. Soc. 146 (1999) 2049-2053.

[40] Stephen J. Paddison, Reginald Paul, T.A. Zawodzinski Jr., A Statistical Mechanical Model of Proton and Water Transport in a Proton Exchange Membrane, J. Electrochem. Soc. 147 (2000) 617-626.

[41] G.J. Elfring, H. Struchtrup, Thermodynamic Considerations on the Stability of Water in Nafion, J. Membr. Sci. 297 (2007) 190-198.

[42] I. Müller, W. Weiss, Entropy and Energy: A Universal Competition, Springer-Verlag, Berlin Heidelberg 2005

[43] I. Müller, Thermodynamics, Pitman, Boston, MA 1985.

[44] A. Morro, I. Müller, A study of swelling and collapse of polyelectrolyte gels, Rheol. Acta 27 (1988) 44-51.

[45] A. Bensberg, Swelling and shrinking of polyacid gels, Continuum Mech. Thermodyn. 9 (1997) 323-340.

[46] P.J. Flory, Principles of Polymer Chemistry, Cornell University Press, Ithaca and London 1953.

[47] A. Bejan, Advanced Engineering Thermodynamics, John Wiley and Songs, New York, NY 1997.

[48] G.M. Gusler, Y. Cohen, Equilibrium Swelling of Highly Cross-Linked Polymeric Resins, Ind. Eng. Chem. Res. 33 (1994) 2345-2357.

[49] H.B. Park, C. H. Lee, J. Y. Sohn, Y. M. Lee, B.D. Freeman, H. J. Kim, Effect of crosslinked chain length in sulfonated polimide membranes on water sorption, proton conduction, and methanol permeation properties, J. Membr. Sci. 285 (2006) 432-443.

[50] S.A.Safran, Statistical Thermodynamics of Surfaces, Interfaces, and Membranes, Addison-Wesley, Reading, MA 1994.

[51] R. Evans, U.M.B. Marconi, Fluids in narrow pores: Adsorption, capillary condensation, and critical points, J. Chem. Phys. 84 (1986) 4.

[52] T.A. Zawodzinski Jr., S. Gottesfeld, S. Shoichet, T.J. McCarthy, The contact angle between water and the surface of perfluorosulphonic acid membranes, J. Appl. Electrochem., 23 (1993) 86-88.

[53] N.H. Jalani, P. Choi, R. Datta, TEOM: A novel technique for investigating sorption in proton-exchange membranes, J. Membr. Sci. 254 (2005) 31-38.

[54] C. Vallieres, D. Winkelmann, D. Roizard, E. Favre, P. Scharfer, M. Kind, On Schroeder's Paradox, J. Membr. Sci. 278 (2006) 357-364.

## Appendix A - Derivation of $a_\theta$ and $b_\theta$

The area of the ends of the liquid columns in the pores can be computed by

$$A = \int_{s_0}^{s_r} \int_{0}^{2\pi} x d\varphi ds \tag{A.1}$$

with $S = \alpha R$, $x = R\sin(\alpha)$, A.1 then becomes

$$A = \int_{0}^{\alpha_1} \int_{0}^{2\pi} R^2 \sin(\alpha)\, d\varphi d\alpha. \tag{A.2}$$

Now relating to contact angle and pore radius $\alpha_1 = \theta - \pi/2$, and $r = R\sin(\alpha_1)$ we get

$$A = \pi r^2 \frac{2}{1+\sin\theta}. \tag{A.3}$$

We define

$$a_\theta(\theta) = \frac{2}{1+\sin\theta}. \tag{A.4}$$

The volume of the ends can be computed by integrating an 'ice cream' cone and subtracting off the cone

$$V_{end} = \int_{0}^{2\pi} \int_{0}^{\alpha_1} \int_{0}^{R} \rho^2 \sin(\phi)\, d\rho d\phi d\theta - \frac{1}{3}\pi r^2 h \tag{A.5}$$

which gives

$$V_{end} = \frac{2}{3}\pi R^3 [1 - \cos(\alpha_1)] - \frac{1}{3}\pi r^2 R \cos(\alpha_1) \tag{A.6}$$

which reduces to

$$V_{end} = \frac{1}{3}\pi r^3 \left\{2\sec^3(\theta)[\sin(\theta) - 1] + \tan(\theta)\right\}. \tag{A.7}$$

We define

$$b_\theta(\theta) = 2\sec^3(\theta)[\sin(\theta) - 1] + \tan(\theta) \tag{A.8}$$

# Appendix B - A Priori Incompressibility

We fix another variable by assuming that water is incompressible $v_l = const.$, therefore the volume of liquid is proportional to the mass of liquid,

$$V_l = v_l m_l. \tag{B.1}$$

We also assume that the protons are incompressible. Minimizing the total free energy with respect to the mass of liquid, $m_l$, yields

$$\begin{aligned}\frac{\partial \mathcal{G}}{\partial m_l} = f_l + R_l T \ln a_l + m_l \frac{\partial f_l}{\partial v_l}\frac{\partial v_l}{\partial m_l} + m_l R_l T \frac{\partial \ln a_l}{\partial m_l} + \left[f_p + R_p T \ln a_p\right]\frac{\partial m_p}{\partial V_l}\frac{\partial V_l}{\partial m_l} \\ + m_p \frac{\partial f_p}{\partial v_p}\frac{\partial v_p}{\partial m_p}\frac{\partial m_p}{\partial m_l} + m_p R_p T \frac{\partial \ln a_p}{\partial m_l} + \frac{\partial f_p^0}{\partial v_p^0}\frac{\partial v_p^0}{\partial m_p^0}\frac{\partial m_p^0}{\partial m_l} + f_p^0 \frac{\partial m_p^0}{\partial m_l} + f_v \frac{\partial m_v}{\partial m_l} \\ - m_v \frac{\partial f_v}{\partial v_v}\frac{\partial v_v}{\partial m_v} + \frac{\partial F_s}{\partial V_l}\frac{\partial V_l}{\partial m_l} + \frac{\partial F_m}{\partial V_l}\frac{\partial V_l}{\partial m_l} + p\frac{\partial V_l}{\partial m_l} + p\frac{\partial V_p}{\partial m_l} + p\frac{\partial V_p^0}{\partial m_l} = 0.\end{aligned} \tag{B.2}$$

From the incompressibility assumption we know $\partial v_l$, $\partial v_p^0$ and $\partial v_p = 0$ therefore

$$m_l \frac{\partial f_l}{\partial v_l}\frac{\partial v_l}{\partial m_l} = m_p \frac{\partial f_p}{\partial v_p}\frac{\partial v_p}{\partial m_p}\frac{\partial m_p}{\partial m_l} = \frac{\partial f_p^0}{\partial v_p^0}\frac{\partial v_p^0}{\partial m_p^0}\frac{\partial m_p^0}{\partial m_l} = 0. \tag{B.3}$$

Due to the Gibbs-Duhem relation

$$m_l R_l T \frac{\partial \ln a_l}{\partial m_l} + m_p R_p T \frac{\partial \ln a_p}{\partial m_l} = 0 \tag{B.4}$$

Since $dV_p = -dV_p^0$, then

$$p\frac{\partial V_p}{\partial m_l} + p\frac{\partial V_p^0}{\partial m_l} = 0. \tag{B.5}$$

Applying $(B.3)$, $(B.4)$, $(B.5)$ and the Maxwell relation

$$\frac{\partial f_\alpha}{\partial v_\alpha}_{t=const.} = -p_\alpha \tag{B.6}$$

to $(B.2)$ yields

$$\frac{\partial \mathcal{G}}{\partial m_l} = f_l + R_l T \ln a_l + \left[f_p - f_p^0 + R_p T \ln a_p\right] \frac{\partial m_p}{\partial V_l} v_l \\ - f_v - p_v v_v + \frac{\partial F_s}{\partial V_l} v_l + \frac{\partial F_m}{\partial V_l} v_l + p v_l = 0. \tag{B.7}$$

We define the surface pressure,

$$p_s = \frac{\partial F_s}{\partial V_l}\,, \tag{B.8}$$

which is due to the change in surface free energy when to the liquid volume changes, and the membrane pressure,

$$p_m = \frac{\partial F_m}{\partial V_l}\,, \tag{B.9}$$

which is due to the change membrane free energy with a change in liquid volume. We also define a proton pressure

$$p_p = \left(f_p - f_p^0 + R_p T \ln a_p\right) \frac{\partial m_p}{\partial V_l} \tag{B.10}$$

which is the energy required to add more protons to the mixture as the boundary of $V_l$ expands. Therefore (2.23) can be rewritten as

$$f_l + R_l T \ln a_l + \left(p + p_p + p_s + p_m + p_s\right) v_l = f_v + p_v v_v \tag{B.11}$$

Assuming $p + p_p + p_s + p_m + p_s = p_{mix}$ and using the Gibbs free energy $g_\alpha = f_\alpha + p_\alpha v_\alpha$, $(B.7)$ becomes

$$g_l + R_l T \ln a_l = g_v \tag{B.12}$$